



# History of Anvers-Hugo Trough, western Antarctic Peninsula shelf, since the Last Glacial Maximum. Part I: Deglacial history based on new sedimentological and chronological data

Zoë A. Roseby<sup>a, b, c, 1, \*</sup>, James A. Smith<sup>a</sup>, Claus-Dieter Hillenbrand<sup>a</sup>,  
Matthieu J.B. Cartigny<sup>d</sup>, Brad E. Rosenheim<sup>e</sup>, Kelly A. Hogan<sup>a</sup>, Claire S. Allen<sup>a</sup>,  
Amy Leventer<sup>f</sup>, Gerhard Kuhn<sup>g</sup>, Werner Ehrmann<sup>h</sup>, Robert D. Larter<sup>a</sup>

<sup>a</sup> British Antarctic Survey, Cambridge, CB3 0ET, UK

<sup>b</sup> School of Ocean and Earth Science, University of Southampton, Southampton, SO14 3ZH, UK

<sup>c</sup> Marine Geosciences, National Oceanography Centre, Southampton, SO14 3ZH, UK

<sup>d</sup> Department of Geography, Durham University, Durham, DH1 3LE, UK

<sup>e</sup> College of Marine Science, University of South Florida, 140 7th Avenue S, St. Petersburg, FL, 33701, USA

<sup>f</sup> Colgate University, 13 Oak Dr, Hamilton, NY, 13346, USA

<sup>g</sup> Alfred-Wegener-Institut Helmholtz-Zentrum für Polar- und Meeresforschung, Marine Geologie, Am Alten Hafen 26, D-27568, Bremerhaven, Germany

<sup>h</sup> Institute for Geophysics and Geology, University of Leipzig, Talstrasse 35, D-04103, Leipzig, Germany

## ARTICLE INFO

### Article history:

Received 26 November 2021

Received in revised form

11 May 2022

Accepted 26 May 2022

Available online 1 August 2022

Handling Editor: C. O'Cofaigh

### Keywords:

Antarctica

Antarctic Peninsula

Sedimentology-marine cores

Glaciation

Deglaciation

Radiocarbon dating

Last Glacial Maximum

## ABSTRACT

Reconstructing the advance and retreat of past ice sheets provides important long-term context for recent change(s) and enables us to better understand ice sheet responses to forcing mechanisms and external boundary conditions that regulate grounding line retreat. This study applies various radiocarbon dating techniques, guided by a detailed sedimentological analyses, to reconstruct the glacial history of Anvers-Hugo Trough (AHT), one of the largest bathymetric troughs on the western Antarctic Peninsula (WAP) shelf. Existing records from AHT indicate that the expanded Antarctic Peninsula Ice Sheet (APIS) advanced to, or close to, the continental shelf edge during the Last Glacial Maximum (LGM; 23–19 cal kyr BP [ = calibrated kiloyears before present]), with deglaciation of the outer shelf after ~16.3 cal kyr BP. Our new chronological data show that the APIS had retreated to the middle shelf by ~15.7 cal kyr BP. Over this 600-year interval, two large grounding-zone wedges (GZW) were deposited across the middle (GZW2) and inner shelf (GZW3), suggesting that their formation occurred on centennial rather than millennial timescales. Expanded sequences of sub-ice shelf sediments occur seaward of the inner GZW3, which suggests that the grounding line remained stationary for a prolonged period over the middle shelf. Grounding-line retreat rates indicate faster retreat across the outer to middle shelf compared to retreat across the middle to inner shelf. We suggest that variable retreat rates relate to the broad-scale morphology of the trough, which is characterised by a relatively smooth, retrograde seabed on the outer to middle shelf and rugged morphology with a locally landward shallowing bed and deep basin on the inner shelf. A slowdown in retreat rate could also have been promoted by convergent ice flow over the inner shelf and the availability of pinning points associated with bathymetric highs around Anvers Island and Hugo Island.

© 2022 The Authors. Published by Elsevier Ltd. This is an open access article under the CC BY license (<http://creativecommons.org/licenses/by/4.0/>).

\* Corresponding author. School of Ocean and Earth Science, University of Southampton, Southampton, SO14 3ZH, UK.

E-mail address: [rosebyz@tcd.ie](mailto:rosebyz@tcd.ie) (Z.A. Roseby).

<sup>1</sup> Present address: School of Natural Sciences, Trinity College Dublin, Dublin, Ireland.

## 1. Introduction

The Antarctic Peninsula Ice Sheet (APIS) is currently losing mass at an accelerating rate (Paolo et al., 2015; Cook et al., 2016; Rignot et al., 2019). Mass loss is largely a response to ocean-induced melting of marine-terminating glaciers and ice shelves, resulting in their retreat and flow acceleration and drawdown of the APIS

(Cook et al., 2016; Rignot et al., 2019). In addition, ice-shelf thinning and retreat has occurred in tandem with atmospheric warming since the early twentieth century, which has driven increased surface melting and propagated collapse through hydrofracture (Scambos et al., 2004). Whilst these key processes are now well understood, there remains uncertainty about the future evolution of the APIS and particularly its subsequent contribution to sea-level rise. Processes such as marine ice sheet instability and ice-cliff instability (MISI and MICI, respectively) have been hypothesised as the main drivers of rapid ice sheet retreat but have not been observed in Antarctica (MICI) or have been subject to limited observation (MISI) (Schoof, 2007; Joughin et al., 2014; Favier et al., 2014; Rignot et al., 2014; Pollard et al., 2015; DeConto and Pollard, 2016). In this context, data on the advance and retreat of the APIS during previous glacial-interglacial cycles can provide vital insight into the response of grounded ice to a range of drivers, including past episodes of atmospheric and ocean warming, and the influence of a retrograde bed on facilitating rapid retreat. Furthermore, detailed palaeo-glaciological reconstructions provide information about key subglacial processes, for example, the role of subglacial meltwater and sediment deformation in facilitating fast flow, which help to improve our understanding of glacier dynamics (e.g., Ó Cofaigh et al., 2005; Kirkham et al., 2019; Larter et al., 2019; Greenwood et al., 2021). Ultimately, this evidence can then be used to validate ice sheet models, thereby improving their ability to accurately predict future changes (e.g., King et al., 2012; Whitehouse et al., 2012a, 2012b; Briggs and Tarasov, 2013; Bracegirdle et al., 2019; Siegert et al., 2020).

Several factors currently limit our ability to accurately reconstruct past glacier dynamics. Principal among these is reliable dating of past changes, because without this it is difficult to assess rates and drivers of change. Accelerator mass spectrometry (AMS)  $^{14}\text{C}$  dating of calcareous (micro-)fossils is considered to provide the most reliable ages from Antarctic shelf sediments over the last 40 kys (e.g. Andrews et al., 1999; Heroy and Anderson, 2005, 2007; Hillenbrand et al., 2010a; Ó Cofaigh et al., 2014), although the scarcity of calcareous (micro-)fossils in Antarctic shelf sediments means that alternative dating methods are often applied, e.g., dating of the acid insoluble organic matter (AIO) fraction of (bulk) sediments (Licht et al., 1998; Andrews et al., 1999; Heroy and Anderson, 2007; Hillenbrand et al., 2010a, 2010b; Smith et al., 2011). The AIO fraction can be “contaminated” by reworked fossil organic carbon that is eroded and transported offshore by ice streams and outlet glaciers (Andrews et al., 1999; Hillenbrand et al., 2010a). This problem is particularly acute in transitional environments, between grounding line retreat and the onset of seasonally open-marine conditions, where the input of fresh organic carbon (from primary productivity in the water column) is low, whilst the supply of detritus eroded and transported by the glacier, which may include fossil organic matter, is high (Domack, 1992). To overcome these limitations, several studies have employed compound specific  $^{14}\text{C}$  dating (Ohkouchi et al., 2003; Yokoyama et al., 2016). Additionally, ramped pyrolysis (RPO)  $^{14}\text{C}$  dating ‘splits’ the bulk sedimentary organic matter into younger, more volatile components and older, more diagenetically stable components using stepped-temperature combustion (Rosenheim et al., 2008). The younger, volatile components are assumed to consist of autochthonous algal-derived organic matter produced in open water and this is reflected in radiocarbon ages that are comparable to those obtained from calcareous (micro-)fossils in the same sediment horizon (Rosenheim et al., 2008; Subt et al., 2017). The RPO method offers great promise for establishing robust palaeo-reconstructions – and in combination with other dating approaches – allows us to place the recent ice sheet changes into a long-term context and, ultimately, provide validation for predictive ice sheet models.

In this study, we apply several radiocarbon dating methods and detailed sedimentological analyses to reconstruct the glacial history of Anvers-Hugo Trough (AHT) on the western Antarctic Peninsula (WAP) shelf (Fig. 1) since the Last Glacial Maximum (LGM; 23–19 cal kyr BP). AHT is one of the best-surveyed palaeo-ice stream troughs in Antarctica (Domack et al., 2006; Lavoie et al., 2015; Larter et al., 2019) and this extensive geophysical data set allowed targeted sediment coring within a known geomorphic setting.

## 2. Regional setting and previous work

The Antarctic Peninsula consists of a central spine of mountains, with a plateau 1800–2000 m above modern sea level, covered by the APIS with ice up to 500 m thick. Today, the APIS is drained by a series of marine-terminating glaciers, some of which form floating ice shelves (e.g., Cook and Vaughan, 2010; Cook et al., 2016). AHT is oriented N–S and extends from the WAP coast to the edge of the continental shelf (Fig. 1). AHT is approximately 144 km long and 24–40 km wide and has been eroded by the repeated advance of the APIS over multiple glacial cycles (Larter et al., 1997; Barker and Camerlenghi, 2002). Water depths within AHT generally increase landwards, from 370 to 440 m at the shelf edge to 550–700 m on the middle shelf (Fig. 2a–b; Pudsey et al., 1994; Livingstone et al., 2012; Larter et al., 2019). On the middle shelf, AHT is oriented NNW–SSE and coalesces with a tributary trough extending from Dallmann Bay (Fig. 1b) (Lavoie et al., 2015), referred to as “Perrier Trough” by Larter et al. (2019). The rugged inner shelf has water depths down to 1400 m, e.g., in Palmer Deep, and features streamlined bedrock, meltwater channels and interconnected basins (Domack et al., 2006; Larter et al., 2019). Geophysical data indicate that the seabed of inner AHT is characterised by outcropping bedrock, whilst on the middle and outer shelf prograding sequences of glacial sediments, deposited over multiple episodes of ice sheet advance, occur (Larter and Barker, 1989; Pudsey et al., 1994). The outcropping bedrock of the inner shelf, including a sill separating Palmer Deep from the main AHT, features crescentic scours, anastomosing channels and northward-shoaling valleys, eroded by subglacial water flow over multiple glaciations (see Fig. 1b for location and Fig. 2 in Larter et al., 2019, for detailed multibeam bathymetry). These features have been associated with a subglacial lake within Palmer Deep that formed during, or prior to, the LGM and that experienced several draining events before being completely evacuated (Domack et al., 2006). Larter et al. (2019) suggested that meltwater availability facilitated fast ice stream flow and controlled shear margin positions within AHT. The submarine geomorphology of the middle and outer AHT is dominated by mega-scale glacial lineations (MSGs), highly elongated parallel ridges and grooves formed during ice streaming, and grounding-zone wedges (GZWs), asymmetrical accumulations of sediment deposited when the grounding line temporarily stabilises during episodic ice-stream retreat (Fig. 2) (Pudsey et al., 1994; Larter and Vanneste, 1995; Heroy and Anderson, 2005; Domack et al., 2006; Livingstone et al., 2012; Larter et al., 2019). The extension of MSGs close to the shelf break provides strong evidence that the grounded APIS extended to this position during the LGM (Larter et al., 2019). Following deglaciation, icebergs gouged scour marks into the seabed at depths shallower than ~590 m below modern-day sea level and overprinted glacial bedforms in some places, including the outermost shelf (Pudsey et al., 1994; Heroy and Anderson, 2005). The bathymetric high surrounding Hugo Island, west of AHT, and extending to the shelf break, is thought to have hosted a grounded ice dome during the LGM (Fig. 1b) (Domack et al., 2006; Lavoie et al., 2015). Additional ice domes also may have existed east of AHT (Fig. 1a; Lavoie et al.,

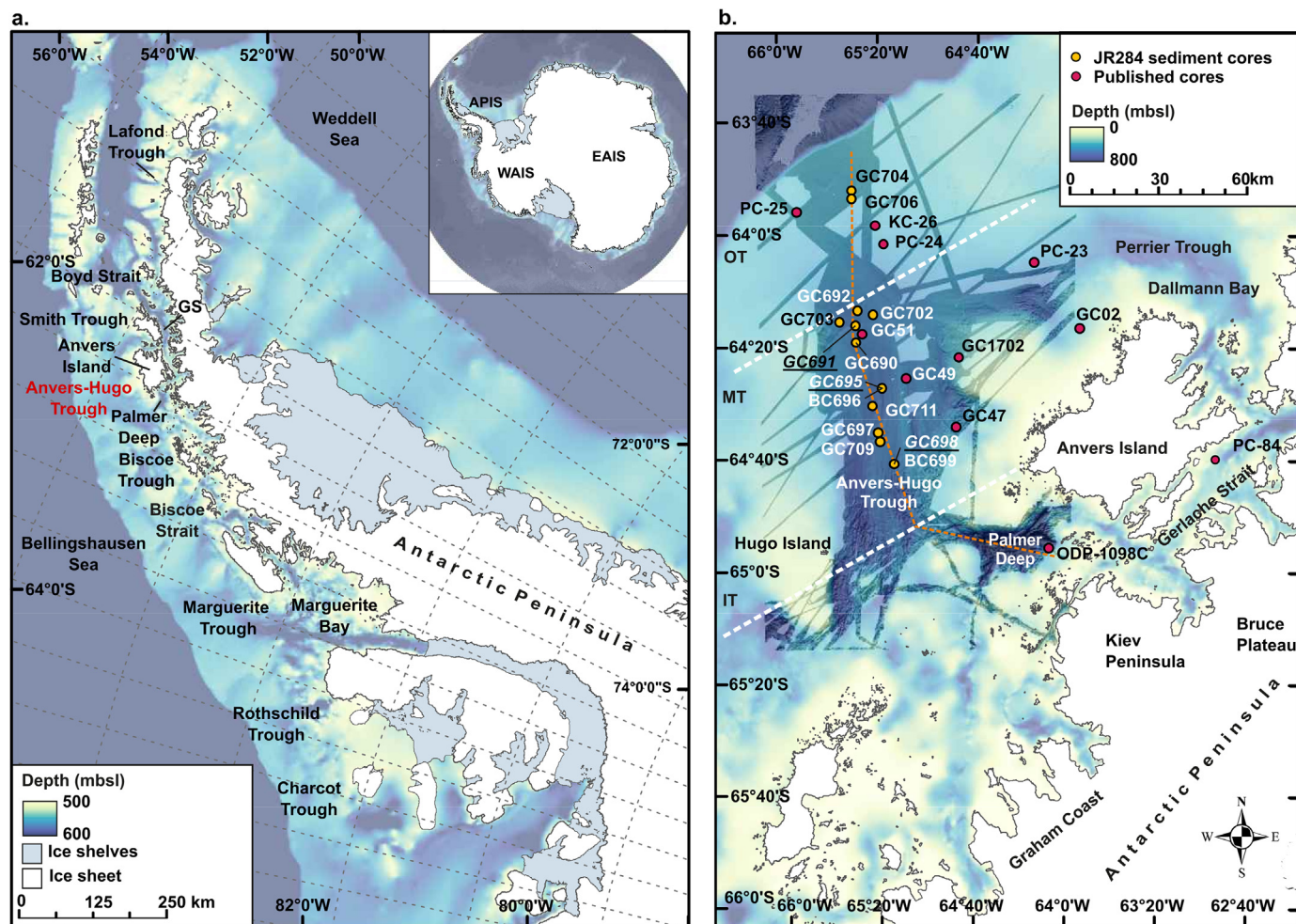


**Fig. 1.** (a) Map of the Antarctic Peninsula showing the location of Anvers-Hugo Trough and other major palaeo-ice stream troughs on the WAP. Gerlache Strait = GS. Regional bathymetry is from Arndt et al. (2013). (b) Detailed map of Anvers-Hugo Trough. White dashed lines indicate the division of the trough into an Outer Trough (OT), Middle Trough (MT) and Inner Trough (IT) region. Red circles denote locations of marine sediment cores with published deglaciation ages (from Harden et al., 1992; Pudsey et al., 1994; Nishimura et al., 1999; Domack et al., 2001; Yoon et al., 2002; Heroy and Anderson, 2005, 2007; Ó Cofaigh et al., 2014). Yellow circles denote JR284 core locations. (For interpretation of the references to colour in this figure legend, the reader is referred to the Web version of this article.)

2015). These ice domes would have constrained and directed ice flow within AHT (Domack et al., 2006; Lavoie et al., 2015).

Available chronological data suggests that deglaciation of the outer shelf was underway by ~16.3 cal kyr BP (KC-26 in Heroy and Anderson, 2007). Note that in this paper, all radiocarbon ages published prior to 2020 were re-calibrated using the updated Marine20 calibration curve and a marine reservoir effect of  $1230 \pm 120$  yrs (Ó Cofaigh et al., 2014), to facilitate comparison with the new ages presented in this study.  $^{14}\text{C}$  ages indicate that the middle shelf was free of grounded ice as early as 13.9 cal kyr BP (GC-1702 in Nishimura et al., 1999). Grounded ice had retreated from Palmer Deep by ~12.9 cal kyr BP (Site 1098 in Fig. 10 of Domack et al., 2006). By ~8.4 cal kyr BP, the Gerlache Strait on the inner shelf (PC83 in Harden et al., 1992) was free of grounded ice (Fig. 1). Except for the outer-shelf minimum deglacial ages, the retreat chronology of the AHT palaeo-ice stream is largely based on the AIO fraction of sediments which, as discussed, can be “contaminated” by reworked fossil organic carbon (Andrews et al., 1999; Hillenbrand et al., 2010a). AIO ages are therefore often considered less reliable than those obtained from calcareous foraminifera tests or other calcareous shells (e.g., Ó Cofaigh et al., 2014). This study aims to improve the deglacial chronology of AHT by applying dating

of calcareous foraminifera and the AIO fraction of (bulk) sediments, together with RPO  $^{14}\text{C}$  dating (Rosenheim et al., 2008), with the application guided by detailed core analysis.

### 3. Methods

#### 3.1. Geophysical data

Extensive marine geological and geophysical data were collected during RRS *James Clark Ross* cruise JR284 in January 2014. Detailed multibeam bathymetric data were collected using the hull-mounted Kongsberg-Simrad EM122, and a TOPAS PS018 parametric echo sounder was used to collect acoustic sub-bottom profiler data (Larter et al., 2019). The JR284 bathymetric data were gridded along with existing multibeam data sets acquired by previous cruises of the RVIB *Nathaniel B. Palmer*, the RRS *James Clark Ross* and HMS *Protector* (Anderson, 2005; Domack, 2005; Lavoie et al., 2015). Gridding was carried out in MB-System software (Caress and Chayes, 1996; Caress et al., 2018), with a grid cell size of 30 m (Larter et al., 2019). The bathymetric grid is available from the UK Polar Data Centre. Bathymetric datasets were visualised and analysed in ArcGIS (ArcMap) by applying various sun illuminations

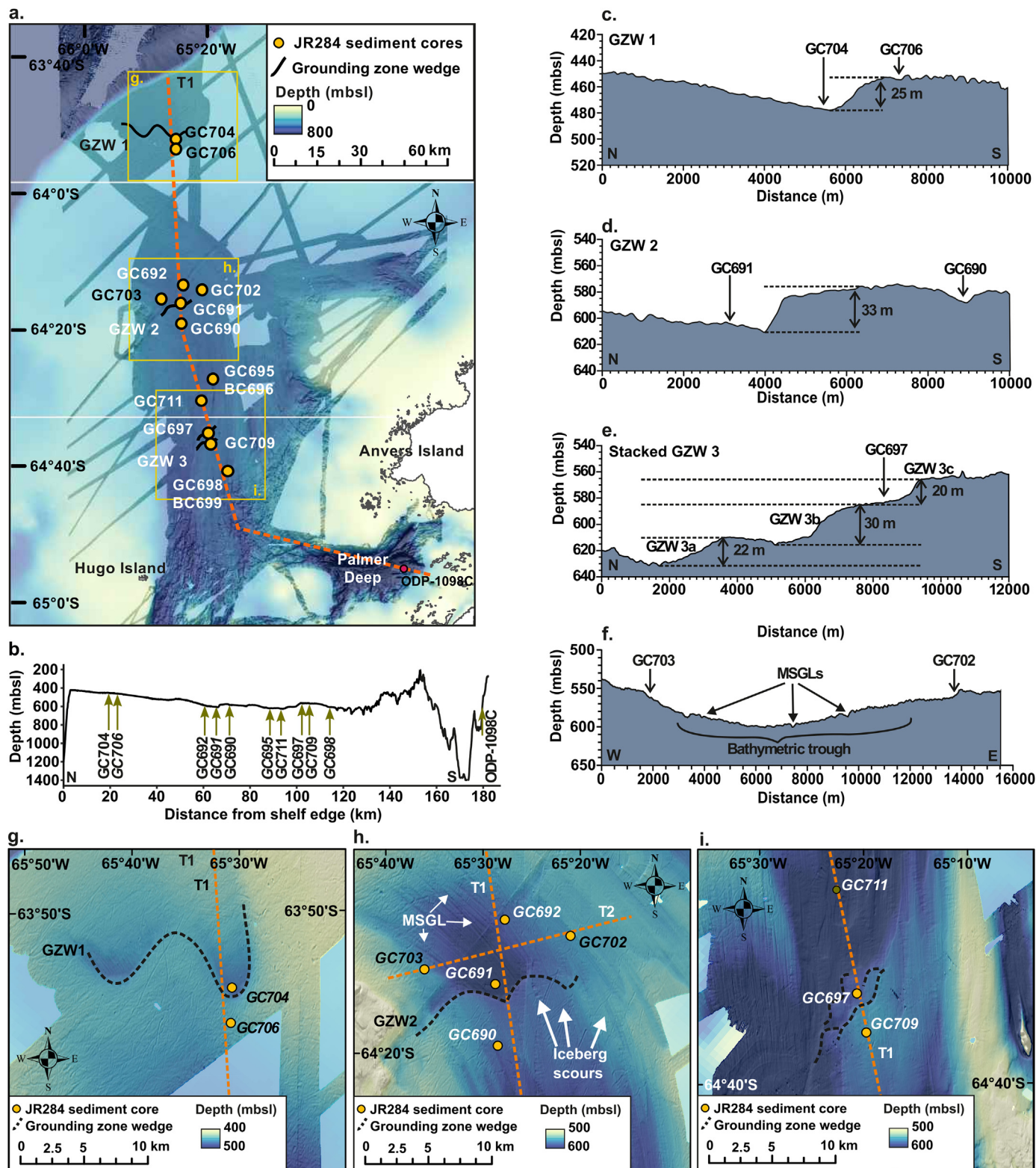


**Fig. 2.** (a) Map of Anvers-Hugo Trough (AHT) with JR284 core locations indicated by yellow circles and the positions of the fronts of GZWs 1–3 by black lines. The dashed orange line indicates the position of the along trough transect T1. (b) Bathymetric profile along trough transect T1 with (projected) core locations, including the position of Palmer Deep core ODP Leg 178 Site 1098 (Domack et al., 2001). (c–e) Bathymetric profiles, core locations and heights of GZW 1 (c), GZW 2 (d) and GZW 3a–c (e). (f) Bathymetric profile of across trough transect T2 with core locations (see panel h for location of profile T2). (g–i) Multibeam coverage of GZW 1 (g), GZW2 (h) and GZW3 (i), with glacial bedforms and sediment core locations (yellow circles). GZW fronts (dashed black lines) and the positions of transects T1 and T2 (dashed orange lines) are also shown. (For interpretation of the references to colour in this figure legend, the reader is referred to the Web version of this article.)

to the data and using 3D Analyst tools to produce bathymetric profiles over glacial landforms and core sites. During JR284, bathymetric and sub-bottom profiler data were used to target core sites to provide the best record of ice-stream retreat in AHT, as outlined below.

### 3.2. Geological data

#### 3.2.1. Sedimentological data

Sediment cores were recovered using the British Antarctic Survey (BAS) 11 cm-diameter gravity corer (GC; NIOZ-type) along two transects, one running along the length of AHT and the other one running across AHT (Table 1). Coring was additionally focussed on three GZWs (GZW 1–3; Fig. 2). Where possible, cores were recovered from the back-slope and seaward pinch-out of each wedge (observed in the multibeam and TOPAS data, respectively) in an attempt to constrain the time-interval over which each GZW formed. A box corer was deployed at most GC sites to recover undisturbed seafloor surface sediments.

Magnetic susceptibility (MS), p-wave velocity and density were measured at 1 cm intervals on un-split whole core sections using a GEOTEK multi-sensor core logger at the British Ocean Sediment Core Research Facility (BOSCORE, Southampton, UK). The core sections were then split, line-scan imaged, described and sampled. Lithological descriptions were based on texture (clay/silt/sand/gravel), structure, colour and contacts between under/overlying units. To refine lithological units and assess sedimentary structures in more detail, a sub-set of archive core halves were X-rayed at Intertek NDT (Derby, UK). Shear strength and water content data were measured every 20 cm down-core to assess sediment compaction and to help, together with other information, such as content of biogenic material and absence/presence of stratification, differentiate between subglacial and glacial marine sediments (e.g., Yoon et al., 1997; Domack et al., 1999; Licht et al., 1999; Evans et al., 2005; Ó Cofaigh et al., 2005; Smith et al., 2009; Hillenbrand et al., 2012). Shear strength was measured using a hand-held shear vane. For water content, 1-cm thick sediment slices were weighed (wet weight), freeze-dried and re-weighed to determine their dry weight. Grain size distribution was determined through wet and dry sieving to separate the mud (<63 µm), sand (63 µm–2 mm) and gravel (>2 mm) fractions. The (dry) mud, sand and gravel fractions were weighed, and these weights were converted into percentages. Biogenic opal, total organic carbon (TOC) and CaCO<sub>3</sub> contents are used in this study as proxies for biological productivity (e.g.,

Domack et al., 1999; Hillenbrand et al., 2010b, 2012; Smith et al., 2014). Biogenic opal content was measured on a subset of cores (Suppl. S1) using the automated leaching method of Müller and Schneider (1993). Determination of diatom abundance and species assemblages was carried out on a qualitative basis through smear slide analysis. Sediments were described as diatom bearing (15–30% diatom content), diatomaceous mud (30–50% diatom content) or diatomaceous ooze (50–100% diatom content), or, as containing trace (<2%), some (5%) or minor (10%) amounts of diatoms.

The opal contents, together with TOC and CaCO<sub>3</sub> contents, were analysed at the Alfred Wegener Institute for Polar and Marine Research (Bremerhaven, Germany). TOC and Total Carbon (TC) were analysed using an ELTRA CS-2000 and Elementar Vario EL III carbon-nitrogen-sulphur analyser, with analytical errors of 3% and 1%, respectively. CaCO<sub>3</sub> was calculated using the equation CaCO<sub>3</sub> = (TC-TOC) × 8.3.

The clay mineral assemblages of a subset of the JR284 sediment cores (Suppl. S1) were analysed by determining the relative contents of chlorite, illite, smectite and kaolinite on the <2 µm grain-size fraction using X-ray diffraction at the Institute for Geophysics and Geology, University of Leipzig, Germany and following the methodology outlined in Ehrmann et al. (1992, 2011). The clay mineral assemblages in Late Cenozoic sediments from the Antarctic continental margin reflect predominantly the source crystalline rocks and source sedimentary strata, from which the detritus was eroded, and the transport pathways of this fine-grained terrigenous detritus (Ehrmann et al., 1992, 2011; Hillenbrand and Ehrmann, 2001; Hillenbrand et al., 2009).

#### 3.2.2. AMS <sup>14</sup>C dating

To constrain the timing of grounding line retreat, dates should be obtained from sediments directly overlying subglacial tills (e.g., Licht et al., 1996; Anderson, 1999; Domack et al., 1999; Heroy and Anderson, 2007; Ó Cofaigh et al., 2014). Identifying the appropriate sediment horizon to date was based on detailed sedimentological and physical properties data. Twenty-seven new ages were acquired for this study; 7 = carbonate (planktic and calcareous benthic foraminifera), 13 = AIO and 7 = RPO <sup>14</sup>C dates. For dating of calcareous foraminifera, sediment samples were sieved at 125 µm and then dried. ~5 mg of foraminifera were then picked from the >125 µm fraction and sent to BETA Analytic, Florida, for dating. Four dates were obtained from planktic foraminifera (*Neogloboquadrina pachyderma* (sin.)), one from calcareous benthic

**Table 1**  
JR284 sediment core ID's, latitude, longitude, water depth (m) and core recovery (m). BC: box core; GC: gravity core.

Core ID	Latitude (°)	Longitude (°)	Water depth (mbsl)	Core Recovery (m)
GC690	-64.337167	-65.489500	584	6.08
BC689	-64.337167	-65.489500	584	0.34
GC691	-64.287333	-65.491500	604	4.10
GC692	-64.243000	-65.478000	578	4.73
BC693	-64.243000	-65.478000	577	0.32
GC695	-64.473833	-65.313000	629	6.74
BC696	-64.473833	-65.313000	628	0.30
GC697	-64.605000	-65.343333	583	7.24
GC698	-64.700000	-65.233333	607	6.34
BC699	-64.700000	-65.233333	605	0.33
GC702	-64.254500	-65.371833	560	4.93
GC703	-64.276667	-65.603500	564	3.86
GC704	-63.886833	-65.511333	475	4.17
BC705	-63.886833	-65.511667	476	0.40
GC706	-63.910833	-65.513833	453	2.38
GC709	-64.632333	-65.330333	556	3.59
BC710	-64.632333	-65.330167	555	0.26
GC711	-64.527333	-65.381333	614	5.88

foraminifera (*Globocassidulina crassa*) and two from mixed planktic and benthic foraminifera (*N. pachyderma* (sin), *Cibicides* spp. and *Fursenkoina fusiformis*).

To constrain the age of post-glacial changes, including the deposition of laminated diatomaceous ooze, we utilised AIO dating. While AIO dating of grounding-line proximal sediments can often yield old AIO ages due to the incorporation of large proportions of re-worked fossil organic matter (Andrews et al., 1999), several studies have shown that sediments with high content of biogenic matter, such as diatomaceous oozes, provide reliable ages (e.g., Andrews et al., 1999; Domack et al., 2001; Leventer et al., 2002; Crosta et al., 2007; Hillenbrand et al., 2010a; Smith et al., 2011; Minzoni et al., 2017). To account for reworked fossil organic carbon that may cause down-core sediments to yield 'old' dates, AIO dating of Antarctic marine sediments routinely involves adjusting for local contamination (Andrews et al., 1999), assuming that the adjustment of ages based on core surface AIO ages is suitable for all depths and lithologic units in the core. However, in some settings, even sediment within the same lithological unit can deviate from this assumption (Rosenheim et al., 2013). A local contamination offset (= surface AIO age – marine reservoir effect) was calculated by dating the AIO of seafloor surface sediments recovered in box cores from the middle shelf (Fig. 1b: BC696, BC699). In addition, paired dating of the AIO fraction and calcareous foraminifera was undertaken in two down-core intervals (445 cm sub-bottom depth in core GC698 and 541 cm depth in core GC695) to test the reliability of AIO ages and suitability of the local contamination offset for correcting down-core AIO ages. For AIO dating, approximately 10–15 g of wet bulk sediment was submitted to BETA Analytic.

Samples for RPO  $^{14}\text{C}$  dating were prepared at the College of Marine Sciences, University of South Florida, following methods outlined in Rosenheim et al. (2008, 2013) and Subt et al. (2016). This involved splitting  $\text{CO}_2$  gas into ~10–25  $\mu\text{mol}$  aliquots, termed 'splits', as the sediment was gradually heated and  $\text{CO}_2$  was produced. The  $\text{CO}_2$  was separated from other gases using a series of liquid nitrogen and liquid nitrogen-cooled isopropanol traps and was sealed into pre-combusted, evacuated Pyrex tubes. These Pyrex tubes contained pre-combusted copper oxide and granulated silver; this allowed the  $\text{CO}_2$  gas to be graphitised prior to  $^{14}\text{C}$  dating at the National Ocean Sciences Accelerator Mass Spectrometry Facility, Woods Hole Oceanographic Institution. RPO  $^{14}\text{C}$  ages were corrected for blank contamination (see Suppl. S2 for details). Where samples did not contain enough 'young' organic carbon to be captured in a normal RPO aliquot (~10–15  $\mu\text{mol}$   $\text{CO}_2$ ), a composite RPO technique was applied. This involved applying the RPO method to two samples of sediment taken from the same horizon;  $\text{CO}_2$  obtained from the first split over these two runs was combined to produce ~10–15  $\mu\text{mol}$   $\text{CO}_2$  for  $^{14}\text{C}$  dating (Subt et al., 2017).

All conventional  $^{14}\text{C}$  ages (including previously published ages) were calibrated in Calib v.8.1.0, using the Marine20 calibration curve (Heaton et al., 2020) and a marine reservoir effect of  $1230 \pm 120$  yrs (Ó Cofaigh et al., 2014). All ages are given as uncorrected  $^{14}\text{C}$  years or cal. yrs before present (BP: where 'present' corresponds to A.D. 1950), quoted as the mid-point of the  $2\sigma$  range and rounded to the nearest decade.

## 4. Results and interpretation

### 4.1. Geomorphological context of sediment cores

Near continuous multibeam and sub-bottom profiler data (Larter et al., 2019) has allowed the glacial geomorphology of AHT to be mapped in detail, which provides important bathymetric and stratigraphic context for the sediment cores and aids the

interpretation of subglacial and transitional sediments. The main trough is dominated by MSGs and three well-developed GZWs (GZWs 1–3). GZWs are likely indicative of pauses during grounding line retreat (Ottesen et al., 2008; Dowdeswell et al., 2008; Dowdeswell and Fugelli, 2012) and have often been associated the presence of past ice shelves (King, 1993; Dowdeswell and Fugelli, 2012; Smith et al., 2019), although others have found no clear link between GZWs and the presence or absence of an ice shelf (Simkins et al., 2018). MSGs extend onto the outer continental shelf (Fig. 2g and see Fig. 4d in Heroy and Anderson, 2005; Larter et al., 2019) and indicate the occurrence and direction of past ice streaming (e.g., Clark, 1993; Ó Cofaigh et al., 2002; Heroy and Anderson, 2005; Larter et al., 2019). In areas shallower than ~590 m water depth (LGM water depth ~470 m), iceberg scours cut across the seafloor both within the trough and on its flanks (Fig. 2g–i). They appear to have eroded the MSGs entirely on the outermost shelf, although MSGs are preserved in deepwater pockets. MSGs are preserved seawards (northwards) of GZWs 1, 2 and 3 and do not overprint them. This indicates that these GZWs were deposited during post-LGM ice-stream retreat from the shelf and were not subsequently overridden by a re-advancing ice stream or reworked by iceberg scouring (Larter et al., 2019). Based on bathymetric profiles, the crest of GZW 1 is 25 m high and that of GZW 2 is 33 m high (Fig. 2c–d); here we define GZW height as vertical height of the crest above the seafloor at the toe of the wedge. The location of GZW 2 coincides with the location of a bathymetric high (Fig. 2h). There is a step-like bathymetry on the mid-shelf caused by the presence of a stacked GZW (Fig. 2e), representing three phases of grounding line still-stands, similar to other stacked GZWs observed on polar continental shelves (Batchelor and Dowdeswell, 2015; Dowdeswell et al., 2016; Arndt et al., 2017; Bart et al., 2017, 2018; Neuhaus et al., 2021). From north to south (GZW 3a–c), the GZWs are 22, 30 and 20 m high respectively.

We identify four acoustic units on TOPAS sub-bottom profiles (A1–4), examples of which are given in two type profiles across several key core sites (GC690, GC691, GC692, GC697; Fig. 3). The regional distribution of unlithified sediments and their acoustic character is the subject of future work and is therefore only briefly described to provide context for the sediment core datasets. A1 is the deepest and therefore the oldest unit, representing the acoustic basement in the area. The character of its upper boundary varies spatially. Where MSGs and iceberg scours are present (e.g., Fig. 3c) the upper boundary of A1 is chaotic, likely because of signal scattering from the grooved surface. Where these landforms are absent, the top reflection of A1 is continuous (e.g., Fig. 3a). Unit A2 is apparently discontinuous in its occurrence by only being present in topographic lows and thinning (onlapping) on to highs. It has a moderate to high amplitude internal character that is weakly and conformably stratified in some places (e.g., Fig. 3a over GZW3a). A3 is an acoustically transparent unit without internal reflections but forms a series of well-defined asymmetric wedges with steep seaward slopes and shallower landward slopes (Fig. 3a and b). A3 is confined to the area of GZW 3b and 3c where it forms a series of back-stepping wedges. A4 is the shallowest unit mapped in AHT and represents the youngest unlithified sediments. It is acoustically transparent with well-defined upper and lower boundaries; A4 has a relatively uniform thickness of about 5 m across AHT. For simplicity, we used a sound velocity of 1500 m/s to convert two-way travel time (ms) into metres (m) subseafloor depth, in order to calculate unit thicknesses on sub-bottom profiles. This is consistent with previous studies in AHT (e.g., Pudsey et al., 1994; Larter and Vanneste, 1995) and with MSCL-derived p-wave velocity measurements from our cores.

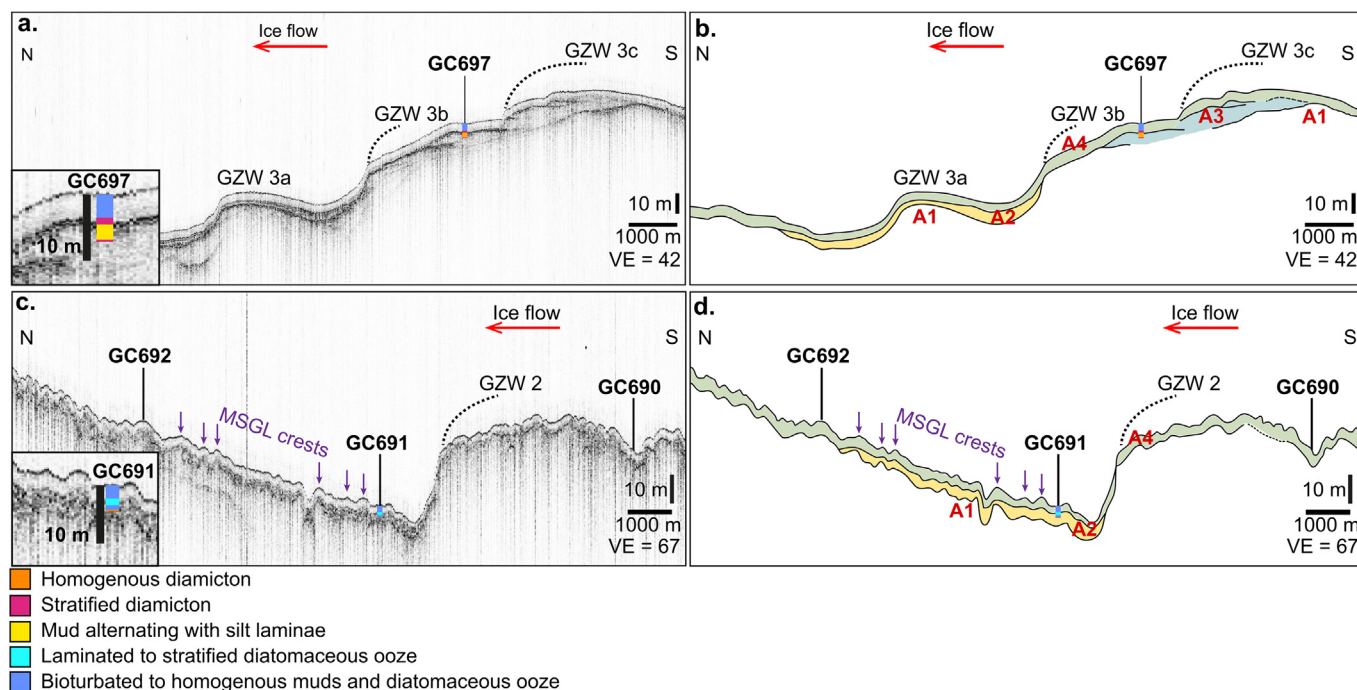


**Fig. 3.** Sub-bottom profiles (TOPAS PS018 parametric echo sounder data) from Anvers-Hugo Trough. (a) N–S profile over GZW 3 (a–c) (see Fig. 2 for location), with log showing summary of core GC697 (note lithological Units 5 and 7 are combined). (b) Schematic drawing highlighting acoustic units (A1–A4) identified in Fig. 3a. (c) N–S profile over GZW 2 (see Fig. 2 for location), with log showing summary of core GC691 (note lithological Units 5 and 7 are combined). (d) Schematic drawing highlighting acoustic units (A1–A4) identified in Fig. 3c.

#### 4.2. Lithological units

Lithological units were defined on the basis of sediment composition, sedimentary structures, X-radiographs and multi-proxy datasets (Figs. 4–6). Seven lithological units were identified (dominating occurrences from older to younger deposits): (1) homogenous diamiction, (2) stratified diamiction, (3) mud alternating with gravel and sand, (4) mud alternating with silt laminae, (5) bioturbated to homogenous mud with dispersed gravel, (6) laminated to stratified diatomaceous ooze and (7) bioturbated diatomaceous ooze (Table 2).

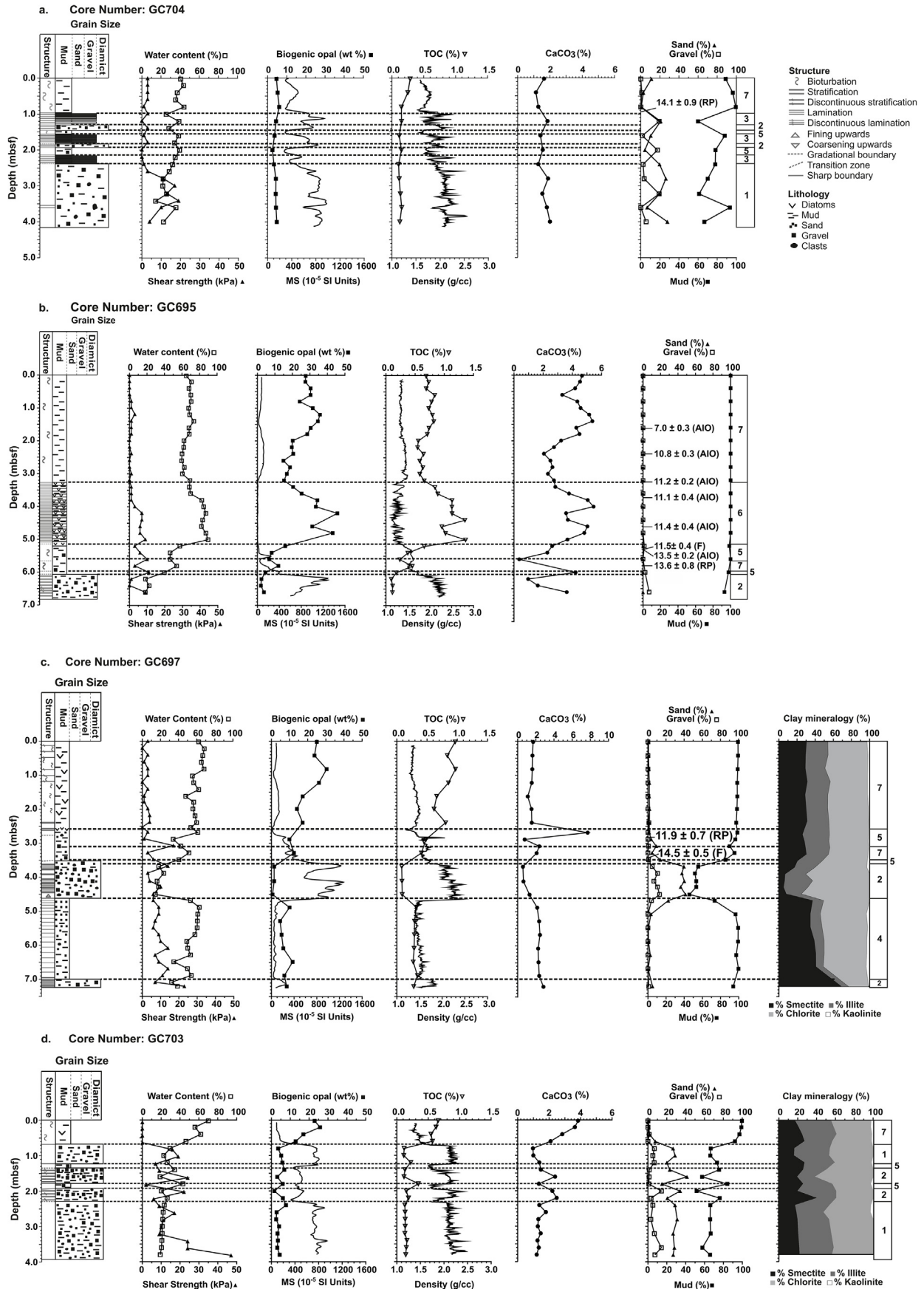
##### 4.2.1. Unit 1: homogenous diamiction

Unit 1 is a homogenous, dark grey, matrix supported diamiction with sub-angular to sub-rounded gravel sized clasts and is present in the lower sections of all sediment cores except GC695 and GC697 (Figs. 4–6 and Table 2). Core GC703, recovered from the shallower western trough flank on the mid-shelf, contains two separate intervals of homogenous diamiction, one at the base and one between 66 and 122 cm (Fig. 4d). Shear strengths typically vary between 10 and 35 kPa in Unit 1, except towards the bases of cores GC690, GC711 and GC703, where shear strength reaches up to 47 kPa (e.g., Fig. 4d). Gravel abundance within Unit 1 varies considerably within and between cores. Contacts with overlying units also vary from sharp to gradational. The clay mineral assemblages of Unit 1 are typically dominated by chlorite with lower contents of smectite and illite and only trace amounts of kaolinite (<1%) (Fig. 4), although there is variation between different core sites and within some Unit 1 diamictions. The bases of GC691 and GC698 have very high chlorite contents (62–64%). Unit 1 of GC690 has high contents of both chlorite and illite (54% and 37% respectively), whilst the sediments close to the base of GC711 are smectite rich (>40%).

The homogenous structure, predominantly terrigenous composition (low biogenic opal, TOC and CaCO<sub>3</sub> contents), low

water contents, high and variable density values and often high shear strength values (Table 2), indicate deposition in a subglacial setting with limited marine influence (e.g., Domack et al., 1999; Licht et al., 1999; Evans and Pudsey, 2002; Ó Cofaigh et al., 2005; Prothro et al., 2018). In most instances, cores containing Unit 1 were recovered from trough areas with MSGLs, features associated with the deformation of ‘soft’ till at the ice stream-sediment interface (Dowdeswell et al., 2004; Ó Cofaigh et al., 2005). Based on the physical properties of Unit 1, and its association with MSGLs, Unit 1 is interpreted as a subglacial deformation till with some alternative explanations (GC706 and GC703). Diatom fragments likely indicate the incorporation/re-working of glaciomarine sediments during ice stream advance (e.g., Ó Cofaigh et al., 2005). Variability in till shear strength is attributed to processes such as lodgement, ploughing and shear deformation, all of which can act simultaneously and are associated with small-scale subglacial hydrologic processes (e.g., sediment permeability, dewatering and meltwater availability) (Ó Cofaigh et al., 2007; Reinardy et al., 2011a, 2011b; Livingstone et al., 2016; Halberstadt et al., 2018).

Core GC706 (Figs. 2g and 5) was recovered from an area characterised by abundant iceberg scours rather than MSGLs. Given the geomorphic context (i.e., proximal to iceberg scours) of GC706 and the fact that iceberg turbates are often indistinguishable from deformation tills (e.g., Hillenbrand et al., 2005), Unit 1 in this core is interpreted as an iceberg turbate. Core GC703 contains two homogenous diamictions, one at the base and one between 66 and 122 cm (Figs. 4d and 5). As with GC706, there are iceberg scour marks proximal to GC703, albeit not as numerous (Fig. 2h). The properties of the lower Unit 1 interval in GC703 (high and variable shear strength, low biogenic and water contents), as well as the stratigraphic position, are compatible with deposition in a subglacial setting. The upper interval of Unit 1 in GC703 could have been deposited as an iceberg turbate, or alternatively as a glaciogenic debris flow deposit, which also shares similar characteristics to



both deformation tills and iceberg turbates (Hillenbrand et al., 2005). The location of GC703 on the sloping flank of AHT (Fig. 2f; 1–1.5° slope) suggests that this core site was likely susceptible to sediment delivery through debris-flow activity.

The clay mineral assemblage of Unit 1 is typically dominated by chlorite and likely derived from source rocks exposed on the inner shelf (Larter et al., 1997; Rebesco et al., 1998) and in Graham Land (British Antarctic Survey, 1981a, 1981b). Basement metamorphic and basic volcanic rocks are thought to be the main source for chlorite in offshore sediments west of the Antarctic Peninsula (Hillenbrand and Ehrmann, 2001; Hillenbrand et al., 2003; Wu et al., 2019). Enrichments of smectite (GC711; Fig. 4d) could reflect increased supply of volcanic detritus from nearby Anvers Island, where Cenozoic volcanic rocks crop out (cf. Pudsey, 2000; Hillenbrand and Ehrmann, 2001). The clay mineral assemblage variability of Unit 1 diamictos within and between cores, is influenced by the spatial distribution of source rock outcrops in relation to the palaeo-ice stream flow line or temporal changes in subglacial transport pathways (Lavoie et al., 2015).

#### 4.2.2. Unit 2: stratified diamicton

Unit 2 is a grey to dark grey stratified, matrix-supported diamicton, present in all but three cores (GC691, GC692, GC706; Table 2). Unit 2 typically forms the basal unit or overlies Unit 1, with some exceptions. In GC697, Unit 2 occurs both at the base and from 360 to 460 cm core-depth (Fig. 4c). In cores GC702, GC703 and GC704 there are multiple Unit 2 intervals interbedded with Unit 5 (Figs. 4d and 5) and, in case of GC704, with Unit 3 (Fig. 5). The thickness of Unit 2 is highly variable, ranging from 10 to 100 cm. The X-radiographs show that Unit 2 is usually crudely stratified (Fig. 6b) and can contain coarser and finer sub-units, as well as mm-scale laminations (Fig. 7). The upper and lower boundaries of Unit 2 are generally gradational, except for the upper intervals of Unit 2 in GC697 and GC703 that have a sharp lower boundary. The clay mineral assemblages of Unit 2 are dominated by variable amounts of chlorite, smectite and illite, with traces of kaolinite (<1%). Like Unit 1, the clay mineral assemblage of Unit 2 varies within and between cores.

The decrease in mud content in Unit 2 relative to Unit 1 indicates an increasing aqueous influence (i.e., marine currents that remove fine particles while the detritus settles through the water column to the seafloor and/or winnow sediments after deposition). The continued presence of coarse sediments suggests proximity to a sediment source, and deposition of Unit 2 at the ice stream grounding line or calving line as a glacial marine diamicton, with some exceptions (Domack and Harris, 1998; Domack et al., 1998, 1999, 2005; Licht et al., 1999; Evans and Pudsey, 2002; Prothro et al., 2018; Hillenbrand et al., 2005, 2010b; Smith et al., 2011, 2014, 2017, 2019). In cores GC711 and GC703 (lower Unit 2 interval) the clay mineral assemblage of Unit 2 differs from the underlying Unit 1 (Fig. 4). Change in sediment provenance of Unit 2, relative to Unit 1, could be attributed to iceberg rafting and deposition of sediments near the calving line, where icebergs can deposit detritus with a different provenance, derived from multiple (distal) sources (Domack and Harris, 1998; Domack et al., 1999; Hillenbrand et al., 2009).

The stratigraphic position of the upper interval of Unit 2 in core

GC697 (360–460 cm) differs from most other cores, in that it does not overly Unit 1. It instead sits between an underlying interval of Unit 4 and an overlying interval of Unit 5. The normal grading of the upper part of Unit 2 in GC697 is indicative of sediment sorting (Fig. 7a). Such sorting could occur at a calving line, where icebergs melt and/or roll-over producing graded deposits (Drewry and Cooper, 1981; Powell, 1984). Alternative explanations for the deposition of the upper part of Unit 2 include grounding line readvance or glaciogenic debris flows. From the sub-bottom profiler data we can see that site GC697 is situated in a trough location that experienced dynamic grounding line retreat, with multiple pauses represented by the deposition of stacked GZW 3 (Fig. 3a). Therefore, it is possible that following initial retreat the grounding line readvanced to site GC697. However, based on the sorting observed, we favour the interpretation that the upper Unit 2 interval in GC697 results from sedimentation at an ice shelf calving line.

In cores GC704 and GC702 there are multiple Unit 2 intervals interbedded with Unit 5 and, in the case of GC704, with Unit 3. This suggests oscillations of the grounding line even at its relatively stable position on GZWs 1 and 2, respectively, resulting in changes from grounding line proximal deposition (Unit 2) to more distal deposition (Unit 5; see below) at the core site, or intermittent deposition by debris flows in front of the GZW. Finally, the upper Unit 2 interval in GC703, recovered from the sloping flank of AHT (Fig. 2h), is considered to represent a glaciogenic debris flow. This unit is sandwiched between two Unit 5 intervals (see below).

#### 4.2.3. Unit 3: mud alternating with gravel and sand

Unit 3 is a laminated to stratified, grey to dark grey mud with mm to cm-thick sand and gravel layers (Figs. 4a and 6c). This unit is exclusively present in core GC704 from the outermost shelf. Sand and gravel contents vary between individual layers. We interpret the sand and gravel layers, within an otherwise muddy unit, to indicate the episodic delivery of coarse material through melt-out of basal debris (Powell, 1984; Powell et al., 1996). Inspection of the X-radiographs reveals that the coarser sand and gravel layers are clast supported, suggesting that fine sediments have been removed during deposition or winnowed after deposition (Fig. 6c). Core GC704 is located near the shelf edge, where high bottom currents are common (Pudsey et al., 1994; Pirrung et al., 2002; Hillenbrand et al., 2010b). Sediment core GC704 was recovered seawards of GZW 1 (Fig. 2a and g) and so the episodic delivery of coarse material is indicative of an oscillating grounding line at a generally stable position.

#### 4.2.4. Unit 4: mud alternating with silt laminae

Unit 4 consists of grey muds that alternate with silt laminae. It is present in cores GC697 and GC698. Within core GC697, Unit 4 is 234 cm thick and sits between two intervals of Unit 2 (Fig. 4c). Within core GC698, Unit 4 is sandwiched between Unit 1 and Unit 2 diamictos (Fig. 5). In both cores, X-radiographs reveal that the laminae are continuous to discontinuous. They are also contorted and occasionally faulted (Fig. 6d and e), which could be the result of either coring disturbance or post-depositional deformation caused by the sedimentation of the overlying Unit 2. Unit 4 additionally shows dispersed gravel-sized clasts, which occasionally “float”

**Fig. 4.** Core lithology and sedimentological data versus depth (in meters below seafloor, mbsf) for cores (a) GC704, (b) GC695, (c) GC697 and (d) GC703. Plots illustrate water content (open squares), shear strength (closed triangles), magnetic susceptibility (MS), biogenic opal (closed squares), TOC (open triangles), CaCO<sub>3</sub> (closed circles), density, contents of mud (<63 μm, closed squares), sand (63 μm–2mm, closed triangles) and gravel (>2 mm, open squares). Clay mineral assemblages are also shown where measured. Sedimentary structures were identified using X-radiographs. Dashed lines indicate the boundaries between lithological units, which are numbered in the boxes on the far right: (1) homogenous diamicton, (2) stratified diamicton, (3) mud alternating with sand and gravel, (4) mud alternating with silt laminae, (5) bioturbated mud with dispersed gravel, (6) laminated to stratified diatomaceous ooze and (7) bioturbated diatomaceous ooze. Calibrated AMS <sup>14</sup>C ages from this study, with ages in cal. kyr BP (F: foraminifera, RP: ramped pyrolysis, AIO: acid insoluble organic material) are also shown. Additional core logs are provided in Supplementary S3.

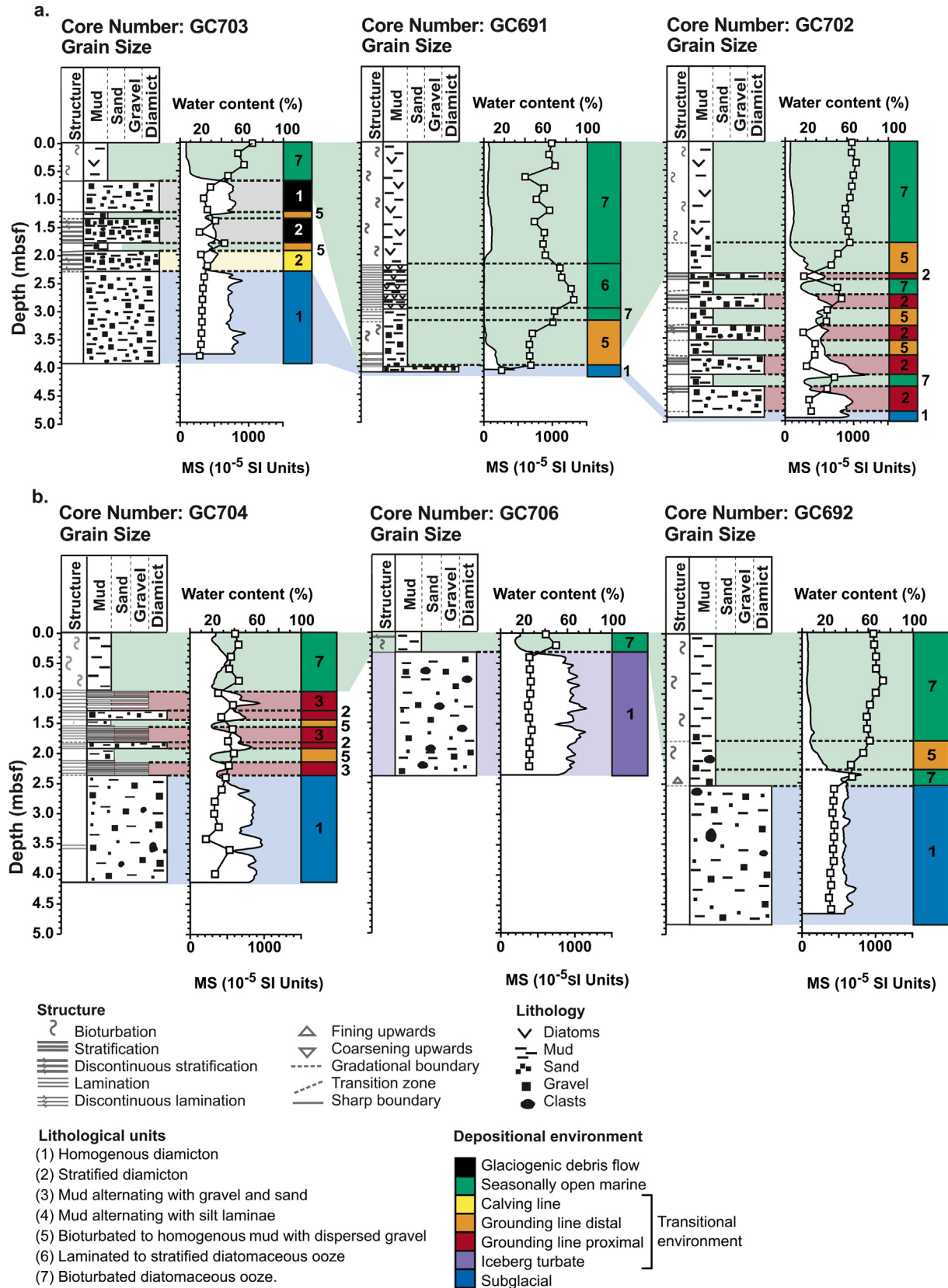


**Fig. 5.** Core panels ((a) Transect T2, located in Fig. 2h, and (b-d) Transect 1, located in Fig. 2a and g-i) summarising the distribution of lithological units within AHT as well as their depositional environments (indicated by colour). Also shown are magnetic susceptibility values (thin black lines) and water contents (open square symbols) for each core. (For interpretation of the references to colour in this figure legend, the reader is referred to the Web version of this article.)

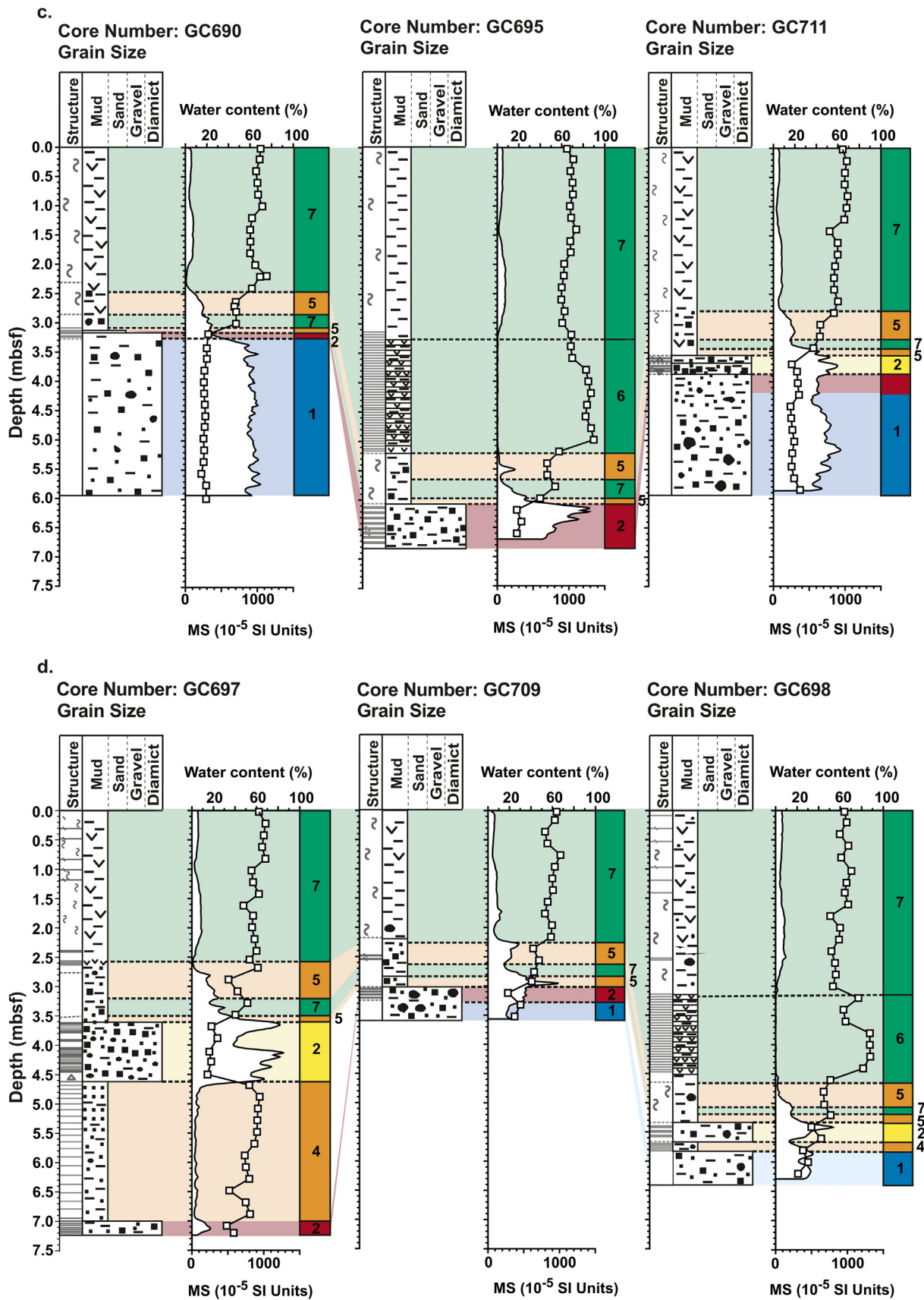
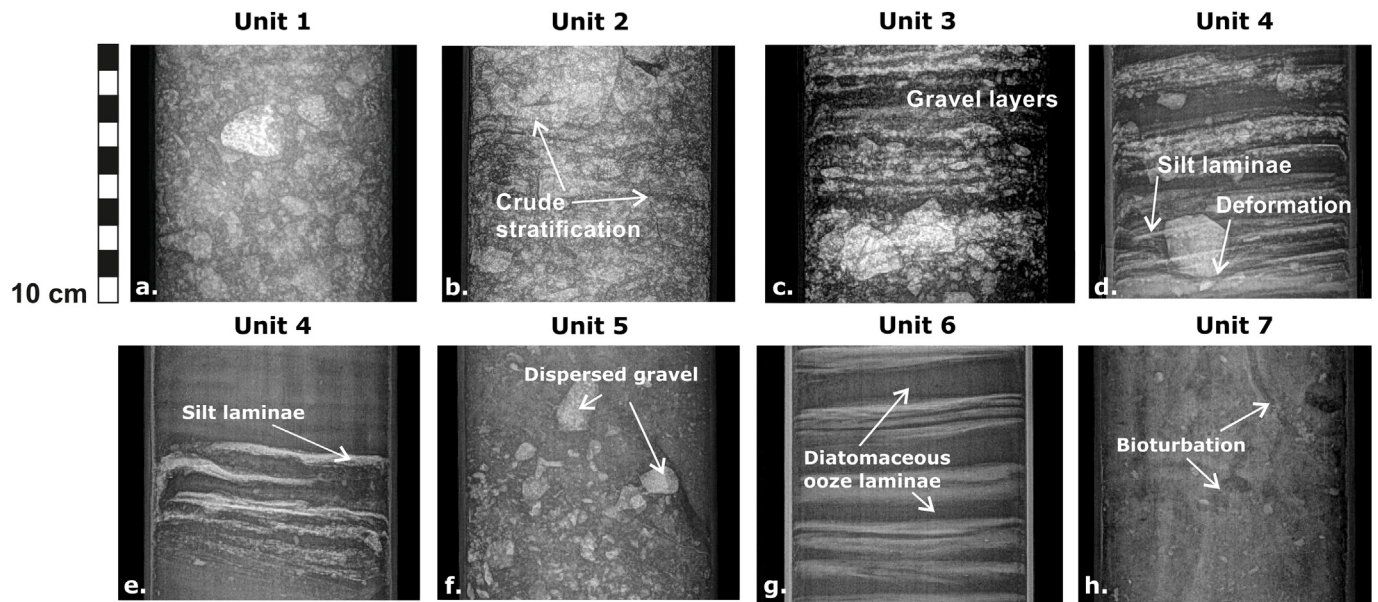


Fig. 5. (continued).



**Fig. 6.** X-radiographs (negatives) showing examples of the lithological units identified in the sediment cores. (a) Unit 1: Homogenous diamicton in core GC690. (b) Unit 2: Stratified diamicton in core GC697. (c) Unit 3: Mud alternating with sand and gravel in core GC704. (d) Unit 4: Mud alternating with silt laminae in core GC698. (e) Unit 4: Mud alternating with silt laminae in core GC697. (f) Unit 5: Bioturbated mud with dispersed gravel in core GC698. (g) Unit 6: Laminated to stratified diatomaceous ooze in core GC691. (h) Unit 7: Bioturbated diatomaceous ooze in core GC704.

**Table 2**

Characteristics of each lithological unit based on water content (%), shear strength (kPa), magnetic susceptibility ( $10^{-5}$  SI Units) and biogenic opal, TOC,  $\text{CaCO}_3$  and diatom content (%). Values are averages for each core.

Unit	Description	Cores present	Water content (%)	Shear strength (kPa)	Magnetic susceptibility ( $10^{-5}$ SI Units)	Biogenic opal content (wt. %)	TOC (wt. %)	$\text{CaCO}_3$ (wt. %)	Microfossil content (%)	Interpretation
1	Homogenous diamicton	GC704, GC706, GC692, GC691, GC690, GC711, GC709, GC698, GC703, GC702	17-26	10-35	401-960	2-4	0.1-0.2	1.1-3.2	2-5	Subglacial deformation till
2	Stratified diamicton	GC704, GC690, GC695, GC711, GC697, GC709, GC698, GC702, GC703	18-38	3-17	70-920	1-6	0.1-0.3	0.8-2.3	2-10	Glacimarine diamicton (grounding line proximal)
3	Mud alternating with gravel and sand	GC704	32-38	~1	250-680	4	0.1-0.2	1.4-1.8	0-5	Grounding line-proximal, winnowed sediment
4	Mud alternating with silt laminae	GC697, GC698	54	9	175	8	0.3	2.3	0-2	Sub-ice shelf plumite, grounding line-distal
5	Bioturbated to homogenous mud with dispersed gravel	GC704, GC692, GC690, GC695, GC711, GC697, GC709, GC698, GC792, GC703	17-55	0-10	76-319	2-10	0.1-0.6	0.4-5.6	20-30	Hemipelagic deposition, low primary productivity
6	Laminated to stratified diatomaceous ooze	GC691, GC695, GC698	76-78	2-5	3-8	28-31	0.8-1	3.5- 4.6	80-100	Hemipelagic deposition, very high diatom productivity
7	Bioturbated diatomaceous ooze	GC704, GC706, GC692, GC692, GC690, GC695, GC711, GC697, GC709, GC698, GC702, GC703	37-67	0-9	71-481	5-26	0.2-0.8	0.1-3.7	50-100	Hemipelagic deposition, high diatom productivity

within and between the laminae and, in some places, contort the laminae (Fig. 6d). The shear strength values and microfossil, biogenic opal, TOC and  $\text{CaCO}_3$  contents of this unit are comparable to those of Units 1–3, but the magnetic susceptibility values are considerably lower, and the water content is higher.

The fine-grained nature of Unit 4 suggests its deposition in a grounding line distal setting (Domack and Harris, 1998). Silt laminae may be introduced through the lateral sorting of sediment-rich meltwater plumes by tidal/ocean currents (Jacobs et al., 2011; Kilfeather et al., 2011; Witus et al., 2014; McKay et al., 2016; Lepp et al., 2022; Smith et al., 2017). The predominantly terrigenous

composition of Unit 4 indicates deposition in a low productivity environment, likely associated with the presence of an ice shelf (Domack and Harris, 1998; Domack et al., 1999; Hillenbrand et al., 2010b; Kilfeather et al., 2011; Witus et al., 2014; Smith et al., 2014, 2017, 2019). Intervals of relatively high biogenic opal (GC697: 11 wt % at 648 cm) and TOC contents (GC697: 0.35 wt % at 688 cm) indicate sporadic advection of biogenic material beneath the ice shelf from the open ocean (Hemer and Harris, 2003; Hemer et al., 2007; Post et al., 2014), or periods of higher surface water productivity in the absence of an ice shelf. The general lack of coarse-grained material is consistent with a grounding line distal

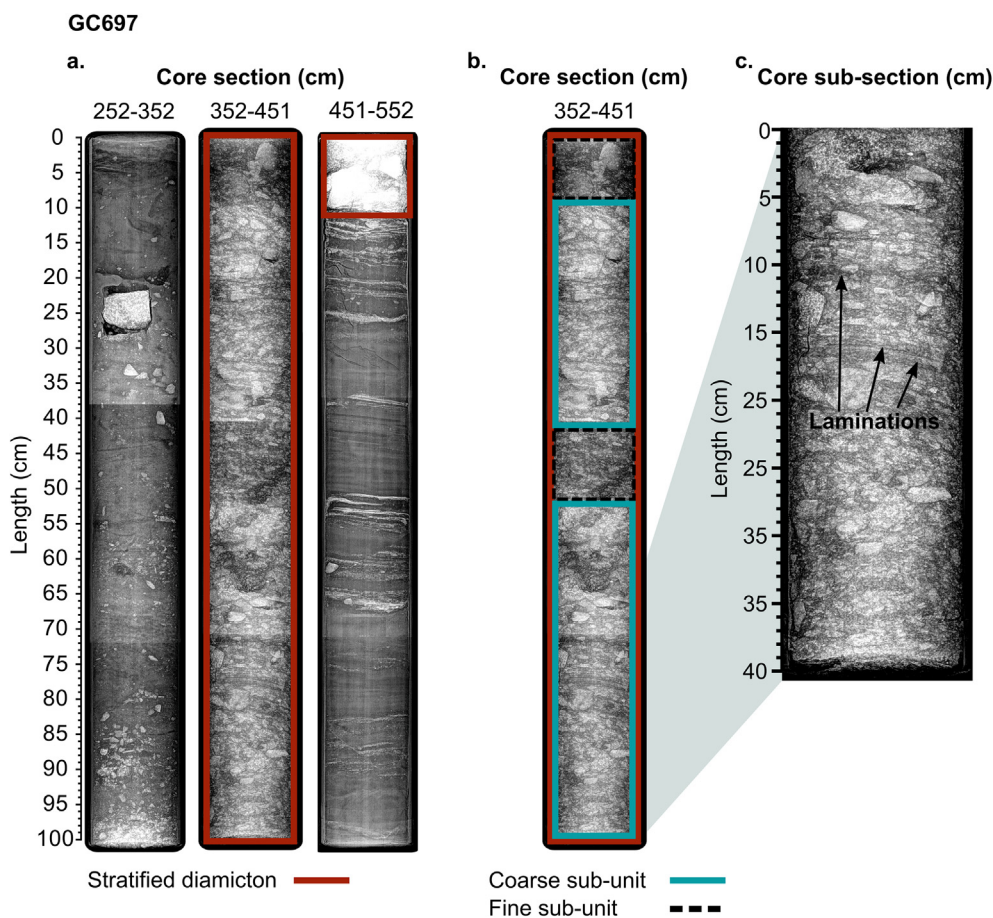


**Fig. 7.** X-radiograph (negatives) of core GC697 illustrating stratification within Unit 2. (a) The whole of Unit 2 (red, solid border; 360–460 cm); including its contacts to underlying Unit 4 and overlying Unit 5. (b) Illustration of coarser-grained (light blue, solid border) and finer-grained (black, dashed border) intervals. (c) The coarser-grained crudely stratified intervals often include millimetre-scale laminations (black arrows). (For interpretation of the references to colour in this figure legend, the reader is referred to the Web version of this article.)

setting, as most basal debris tends to melt out preferentially at the ice shelf base within ~1.5–10 km of the grounding line, although this distance is poorly constrained (Domack and Powell, 2018; Smith et al., 2019). Rare, dispersed gravel-sized clasts in Unit 4 represent ice-rafted debris (IRD), documenting that a few clasts did not melt out proximal to the grounding line but were transported further offshore either within the ice shelf or at its base. In core GC697, Unit 4 is overlain by graded iceberg rafted diamiction, deposited at the calving line as the ice stream/shelf retreated landwards and passed over the core site. In core GC698 Unit 4 is thin (13 cm) relative to Unit 4 in GC697 (234 cm), which suggests that any period of ice shelf cover was relatively brief, or that sedimentation rates were much lower.

#### 4.2.5. Unit 5: bioturbated to homogenous mud with dispersed gravel

Unit 5 is grey, bioturbated to homogenous, diatom-bearing mud with dispersed gravel. Unit 5 is present in most cores (Figs. 4 and 5 and Table 2) and generally has a gradational lower boundary with Unit 2 or 1. Water contents and concentrations of diatoms, biogenic opal, TOC and CaCO<sub>3</sub> are typically higher than in Units 1 and 2 (Fig. 4), and these values generally increase upwards throughout Unit 5, whilst shear strengths and magnetic susceptibilities both decrease up-core. Concentrations of gravel grains (up to 4 cm in size) decrease towards the top of the unit and Unit 5 typically has a gradational upper contact with Unit 7 (Fig. 6f). Unit 5 is generally

dominated by chlorite (~41%), with 29% illite and 29% smectite. The clay mineral assemblage of Unit 5 is similar between cores.

The fine-grained composition of Unit 5 indicates deposition in a grounding line distal setting (Domack and Harris, 1998). The biogenic contents, particularly the diatom component, of this unit are higher than in Units 1–4, which indicates an increasing open-marine influence. However, relative to Units 6 and 7 (see below), Unit 5 is characterised by relatively low biogenic contents (Table 2). Low biogenic contents are related to the presence of a pervasive ice canopy, which suppresses biological production (Maddison et al., 2005; Leventer et al., 2002).

#### 4.2.6. Unit 6: laminated to stratified diatomaceous ooze

Unit 6 is present in cores GC691, GC695 and GC698 and consists of laminated and stratified diatomaceous ooze (Figs. 4b, 5 and 6g). There are 83, 68 and 44 laminae of near-pure (80–100% diatom content) diatomaceous ooze ranging in thickness from 0.1 to 3.7 cm within cores GC695, GC698 and GC691, respectively. *Chaetoceros* subgenus *Hyalochaete* (*Chs*), including vegetative cells and resting spores, dominate the ooze layers. These ooze laminae are generally olive to olive brown and alternate with layers of grey terrigenous mud. The biogenic opal content is surprisingly low (28–31%) when compared to the estimated diatom content from smear slide analyses (80–100%). This may reflect a sampling bias, whereby mud-dier sediments were sampled for biogenic opal or, more likely, an over/under-estimation of diatom/biogenic opal content from the

smear slide analysis and automated leaching technique, respectively (cf. Pudsey, 2002; Hillenbrand et al., 2010a). Despite this over/underestimation, which appears to be pronounced in Units 6 and 7, these techniques are still useful for comparing the relative biogenic contents of sedimentary units. Unit 6 has clay mineral assemblages that are comparable to Unit 5.

Unit 6 is interpreted to have been deposited in a seasonally open-marine setting with extremely productive surface waters. *Chs* resting spores and vegetative cells dominate the ooze layers. This subgenus is associated with early spring conditions, when melting sea ice induces stratification of the water column, concentrating nutrients in the surface waters and promoting high primary productivity (Leventer et al., 2002,2006; Crosta et al., 2004; Maddison et al., 2005; Pike et al., 2008). The layers of grey terrigenous mud are associated with discharge of sediment laden glacial meltwater from glaciers, ice shelves and icebergs (Leventer et al., 2002; Maddison et al., 2005). Previously studied laminated diatomaceous oozes are associated with exceptionally high spring productivity and mass flux of diatoms to the seafloor; such conditions are typical of calving bay re-entrants and laminae can represent annual sedimentation (e.g., Leventer et al., 2002,2006; Maddison et al., 2005, 2006). The formation and deposition of laminated diatomaceous ooze sequences in AHT, and the impact of deglacial processes on biogenic productivity more generally, is discussed further in a companion paper Roseby et al. (in press).

#### 4.2.7. Unit 7: bioturbated diatomaceous ooze

Unit 7 is an olive-green, bioturbated diatomaceous ooze with dispersed gravel-sized grains (Figs. 4, 5 and 6h). Apart from forming the uppermost lithological unit in all cores, it occurs as a thin (18–34 cm) interval between underlying Unit 1 and overlying Unit 5 in cores GC692 and GC691 and is sandwiched between two Unit 5 intervals in cores GC690, GC695, GC711, GC697, GC709 and GC698 (Fig. 5). The diatom content of Unit 7 varies, but is always >50%, with occasional ~3 mm thick intervals of pure diatomaceous ooze. Unit 7 generally contains a mixed diatom assemblage, but the pure ooze intervals are dominated by *Chs* resting spores and vegetative cells. In cores recovered from the outer shelf, Unit 7 is greyer and has lower concentrations of biogenic opal, TOC and CaCO<sub>3</sub>. The thickness of Unit 7 decreases towards the outer shelf. Unit 7 is characterised by similar clay mineral assemblages as found in Units 5 and 6 with 17–37% smectite, 20–45% illite, 30–50% chlorite and 0–6% kaolinite.

The high diatom contents and bioturbation of Unit 7, together with the dispersed gravel grains, which are interpreted as IRD, indicate a seasonally open-marine setting, comparable to modern-day environmental conditions on the Antarctic continental shelf. Variability in the contents of microfossils, biogenic opal, TOC and CaCO<sub>3</sub> over time may reflect temporal changes in oceanographic and/or climatic conditions that promote or diminish diatom bloom events (Maddison et al., 2005; Leventer et al., 2002). Unit 7 generally thins northwards, which is consistent with previous observations of Holocene sediments deposited in AHT and which can be attributed to stronger ocean currents on the outer continental shelf (Pudsey et al., 1994). Glacial discharge introduces sediments to nearshore regions, as well as meltwater and nutrients that promote high productivity in coastal areas (Pudsey et al., 1994; Garibotti et al., 2003; Annett et al., 2015, 2017). These factors additionally contribute to the offshore trend in sediment thickness observed and account for the lower biogenic content of Unit 7 in outer shelf cores (Fig. 4).

### 4.3. AMS <sup>14</sup>C chronology

#### 4.3.1. Local contamination offset

In order to assess the degree to which fossil carbon influences the AIO fraction in AHT, we dated two seafloor surface sediment samples. BC699 and BC696 yielded AIO ages of 2320 ± 30 <sup>14</sup>C yr BP and 2080 ± 30 <sup>14</sup>C yr BP, respectively. Although older than the regional marine reservoir (1230 ± 120 yrs; Ó Cofaigh et al., 2014), the fact that the two ages are similar (separated by only 180–300 years) and not more than 1100 years older than the marine reservoir indicates that the influence of fossil carbon is not as severe as in some other parts of the Antarctic Peninsula shelf (e.g., the area of the former Larsen A and B ice shelves, where core-top sediments yield AIO ages of up to 9360–17,300 <sup>14</sup>C yr BP; Brachfeld et al., 2003; Domack et al., 2005; Pudsey et al., 2006).

#### 4.3.2. Downcore ages: comparisons and corrections

Paired dating of the AIO fraction and calcareous foraminifera was undertaken in two down-core intervals (445 cm sub-bottom depth in core GC698 and 541 cm depth in core GC695) to test the reliability of AIO ages and suitability of the local contamination offset for correcting down-core AIO ages. In core GC698, the two uncorrected <sup>14</sup>C ages (AIO date is 11,390 ± 50 and benthic foraminifera date is 11,220 ± 30 <sup>14</sup>C yrs BP) are in close agreement and differ by just 90–250 years. Their similarity implies that the contamination with fossil carbon during the time of deposition was almost negligible. Importantly, the dates are from the laminated and stratified diatomaceous ooze (Unit 6) with a higher biogenic content (28 wt% biogenic opal content, 0.99 wt% TOC content and 1.3 wt% CaCO<sub>3</sub> content) than the dated surface sediment in BC699 from the same site (21 wt% biogenic opal content, 0.79 wt% TOC content and 1.1 wt% CaCO<sub>3</sub> content). The similarity in the two <sup>14</sup>C ages at 445–446 cm depth in GC698 is attributed to the high diatom and TOC contents of the laminated diatomaceous ooze and is consistent with previous work that suggested that reliable AIO dates can be obtained from sediments with high biogenic content i.e., diatomaceous oozes (e.g., Andrews et al., 1999; Hillenbrand et al., 2010a). Consequently, we follow Hillenbrand et al. (2010a) by correcting ages derived from diatomaceous oozes (Unit 6) by subtracting the marine reservoir effect only (i.e., no local contamination offset correction is applied). This assumes that all the laminated diatomaceous ooze intervals were largely unaffected by deposition of reworked fossil organic matter, consistent with work showing that local contamination offset corrections can vary through lithologic units (Rosenheim et al., 2013).

In contrast, the uncorrected AIO age in core GC695 (541–542 cm; Unit 5) is 13,690 ± 30 <sup>14</sup>C yrs BP, whilst the planktic foraminifera derived age is 11,100 ± 40 <sup>14</sup>C yrs BP (Suppl. S5). The age-offset between the two ages, even if the AIO date is corrected for a local contamination offset of 850 yrs, highlights the difficulty in relying solely on the AIO fraction. In this case, the discrepancy appears to be a consequence of the predominantly terrigenous composition of the sample (biogenic opal = 8 wt %, TOC = 0.38 wt %, CaCO<sub>3</sub> = 0.65 wt %), which has the lowest biogenic content of all the dated AIO samples in this study. It should also be noted that the sample in GC695 was taken from bioturbated mud with dispersed gravel (Unit 5), which is associated with deposition in a grounding-line distal setting. This sample is therefore more likely to include a significant input of reworked fossil carbon than biogenic-rich sediments. Thus, in this case, the foraminifera date is considered to provide the most reliable age for the deposition of this sediment interval and the AIO date is dismissed.

We employed RPO <sup>14</sup>C preparation techniques (Rosenheim et al., 2008), when foraminifera were absent at sediment horizons of interest, in an attempt to overcome the issues associated with AIO

dating outlined above. In core GC704 the first CO<sub>2</sub> split recovered was dated to  $31.5 \pm 3.5$  <sup>14</sup>C kyr BP using the RPO technique (Suppl. S4). This date is significantly older than the date of the second split, which was  $13.2 \pm 0.3$  <sup>14</sup>C kyr BP. The result from the first split is assumed anomalous and is attributed to an error in sample processing and the date of the second split is reported for this horizon. More generally, the RPO <sup>14</sup>C dates of the first and second CO<sub>2</sub> splits are typically separated by less than 2 kyr and the age of the youngest split is reported (Table 3), as we assume that this represents sediments without contamination by reworked fossil organic carbon. In core GC690, the RPO <sup>14</sup>C age (14.5 cal kyr BP) is younger than the overlying foraminifera age (15.1 cal kyr BP); although these dates are within error. Previous studies have observed that, in some cases, low temperature RPO <sup>14</sup>C ages are younger than carbonate <sup>14</sup>C ages from the same stratigraphic interval (Subt et al., 2016, 2017). The disparity might reflect bioturbation, introducing younger sediments to a particular stratigraphic interval or reworking of 'older' foraminifera (Domack et al., 1999; Subt et al., 2017).

#### 4.3.3. Criteria for selecting deglacial ages

As previously noted, our dating strategy (and assessment of 'reliability') is largely based on previous work (e.g., Ó Cofaigh et al., 2014). Thus, in most instances, <sup>14</sup>C ages obtained from calcareous foraminifera are considered to be the most reliable for constraining ice sheet retreat, followed by RPO and AIO ages derived from diatomaceous oozes. More generally, deglacial ages are primarily obtained from sediments directly overlying subglacial and/or grounding-line proximal sediments (Units 5–7). As such, these dates provide a minimum age of grounding line retreat for each core site (Fig. 8b). In some instances, <sup>14</sup>C ages were rejected from our deglacial chronology because they were derived from 'unreliable' stratigraphies; i.e., the RPO <sup>14</sup>C age from GC706 was recovered from sediments overlying an iceberg turbate and is young

( $12.2 \pm 0.5$  cal kyr BP), relative to a nearby foraminiferal age (KC26:  $16.3 \pm 0.6$  cal kyr BP; Heroy and Anderson, 2007). Similarly, the RPO <sup>14</sup>C date from GC704 is also rejected as being too young ( $14.1 \pm 0.9$  cal kyr BP). GC704 was recovered seawards of GZW 1, in an area that must have deglaciated prior to, or around the same time as, nearby site KC26 ( $16.3 \pm 0.6$  cal kyr BP). Fig. 8a presents all <sup>14</sup>C ages generated as part of this study, while Fig. 8b only shows those relating to deglaciation and considered reliable based on the criteria outlined above. Note that the majority of ages omitted are from post-glacial sediments and were primarily obtained to (a) assess down-core consistency of <sup>14</sup>C ages, and/or to (b) provide age-constraints for changes in environmental conditions following deglaciation (Fig. 8a). These dates, along with quantitative diatom abundance and assemblage data, are utilised in Roseby et al. (in press) to discuss palaeo-productivity and palaeoceanographic changes during the Last Glacial Transition.

## 5. Discussion

### 5.1. Depositional environments in AHT during deglaciation

On the basis of our sedimentological and multi-proxy data, we identify seven depositional environments (Figs. 5 and 9) which document the retreat of grounded ice across AHT. At the LGM, grounded ice had extended to, or very close to, the shelf break, based on the presence of MSGL (Larter and Vanneste, 1995; Larter et al., 2019) and corresponding subglacial till (Unit 1) in core GC704. The subglacial tills documented in this study (Fig. 5; GC704, GC692, GC690, GC711, GC709, GC698, GC702 and GC703), as well as reported from previously published cores from the study area (Pudsey et al., 1994; Heroy and Anderson, 2005), are typically 'soft' (shear strength 10 and 35 kPa) and are likely to be associated with a highly mobile, deforming bed; an interpretation supported by the proximity of these cores to MSGLs (Ó Cofaigh et al., 2005). Higher

**Table 3**

Site information and uncorrected and calibrated AMS <sup>14</sup>C dates for Anvers-Hugo Trough, including sample depth, sampled material/method (AIO: acid insoluble organic material, F: foraminifera, P: planktic, B: benthic, S: shell and RP: ramped pyrolysis), biogenic opal content of sediment and sediment unit dated. SD: stratified diamicton, hbGM: homogenous to bioturbated mud with dispersed gravel, bDO: bioturbated diatomaceous ooze, LDO: laminated to stratified diatomaceous ooze, IT: iceberg turbate. All dates are calibrated in Calib v.8.1.0, using the Marine20 calibration curve. Reported ages are the midpoint between the 2σ standard deviation.

Core	<sup>14</sup> C Lab code	Cruise	Study	Latitude (°)	Longitude (°)	Water depth (m)	Depth Interval (cm)	<sup>14</sup> C age (yr BP)	+/- (yrs)	MRE (yrs)	+/- (yrs)	Core top (yr BP)	LCO (yrs)	Mean calibrated age (yr BP)	+/- (yrs)	Material/Method	Sediment type dated	Biogenic opal (wt. %)
GC690	BETA-442251	JR284	This study	-64.337167	-65.489500	584	307-308	13910	50	1230	120	-	-	15100	450	F (P & B)	bDO	
GC690	OS-134431	JR284	This study	-64.337167	-65.489500	584	313-314	13530	290	1230	120	-	-	14500	900	RP	hbGM	
GC691	BETA-499883	JR284	This study	-64.287333	-65.491500	604	265-266	9520	50	1230	120	-	0	9300	350	AIO	LDO	31
GC691	BETA-442252	JR284	This study	-64.287333	-65.491500	604	285-286	11030	40	1230	120	-	-	11400	400	F (P)	LDO	
GC691	BETA-499884	JR284	This study	-64.287333	-65.491500	604	292.5-293.5	11140	40	1230	120	-	0	11500	400	AIO	LDO	33
GC691	OS-134427	JR284	This study	-64.287333	-65.491500	604	327-328	11260	170	1230	120	-	-	11800	600	RP	bDO	
GC695	BETA-524296	JR284	This study	-64.473833	-65.313000	629	161-162	8250	30	1230	120	-	0	7900	300	AIO	bDO	30
GC695	BETA-524297	JR284	This study	-64.473833	-65.313000	629	240-241	11420	30	1230	120	2080	850	10800	250	AIO	bDO	20
GC695	BETA-493184	JR284	This study	-64.473833	-65.313000	629	324-325	11790	40	1230	120	2080	850	11200	200	AIO	LDO	15
GC695	BETA-493185	JR284	This study	-64.473833	-65.313000	629	372-373	10660	40	1230	120	-	0	11100	400	AIO	LDO	34
GC695	BETA-493186	JR284	This study	-64.473833	-65.313000	629	460.5-461.5	11060	40	1230	120	-	0	11400	400	AIO	LDO	31
GC695	BETA-442253	JR284	This study	-64.473833	-65.313000	629	541-542	11100	40	1230	120	-	-	11500	400	F (P)	hbGM	
GC695	BETA-442249	JR284	This study	-64.473833	-65.313000	629	541-542	13690	30	1230	120	2080	850	13500	200	AIO	hbGM	8
GC695	OS-134419	JR284	This study	-64.473833	-65.313000	629	580-581	12850	290	1230	120	-	-	13800	800	RP	bDO	
BC696	BETA-524298	JR284	This study	-64.473833	-65.313000	629	0	2080	30	1230	120	-	-	-	800	AIO	bDO	28
GC697	OS-134439	JR284	This study	-64.605000	-65.343333	583	281-282	11380	210	1230	120	-	-	11900	650	RP	hbGM	
GC697	BETA-442254	JR284	This study	-64.605000	-65.343333	583	343.5-344.5	13980	40	1230	120	-	-	14500	400	F (P & B)	bDO	
GC698	BETA-499885	JR284	This study	-64.700000	-65.233333	607	365.5-366.5	10570	40	1230	120	2320	1090	9300	200	AIO	LDO	21
GC698	BETA-499886	JR284	This study	-64.700000	-65.233333	607	389-399	10420	40	1230	120	-	0	10500	400	AIO	LDO	33
GC698	BETA-442255	JR284	This study	-64.700000	-65.233333	607	445-446	11220	30	1230	120	-	-	11600	400	F (B)	LDO	
GC698	BETA-442250	JR284	This study	-64.700000	-65.233333	607	445-446	11390	50	1230	120	-	0	11900	450	AIO	LDO	28
BC699	BETA-442248	JR284	This study	-64.700000	-65.233333	606	Surface	2320	30	1230	120	-	-	-	400	AIO	bDO	21
GC704	OS-134424	JR284	This study	-63.868833	-65.511333	475	93-94	13180	290	1230	120	-	-	14100	850	RP	bDO	
GC706	OS-134609	JR284	This study	-63.910833	-65.513833	453	32-33	11770	120	1230	120	-	-	12200	450	RP	IT	
GC709	OS-134443	JR284	This study	-64.632333	-65.330333	556	232-233	10600	220	1230	120	-	-	11000	750	RP	hbGM	
GC709	BETA-442256	JR284	This study	-64.632333	-65.330333	556	284.5-285.5	14410	40	1230	120	-	-	15700	400	F (P)	hbGM	
GC711	BETA-442257	JR284	This study	-64.527333	-65.381333	614	346.5-347.5	14260	40	1230	120	-	-	15500	400	F (P)	hbGM	
PC-23	NBP-0201	Heroy & Anderson 2007		-64.084445	-64.277570	533	306	11170	81	1230	120	-	-	11600	900	S	SD	
PC-24	NBP-0201	Heroy & Anderson 2007		-64.046476	-65.297234	557	190	14020	110	1230	120	-	-	15200	1000	F (P & B)	SD	
PC-25	NBP-0201	Heroy & Anderson 2007		-63.949026	-65.883094	438	20-30	14450	120	1230	120	-	-	15800	1000	F (P & B)	SD	
KC-26	NBP-0201	Heroy & Anderson 2007		-63.991068	-65.355262	530	248-252	14880	200	1230	120	-	-	16300	1200	F (P & B)	IT	
GC-02	KARP 98/99	Yoon et al. 2002		-64.291822	-63.962336	400	70	12840	85	1230	120	3000	1770	11200	600	AIO	hbGM	
GC49	D172	Pudsey et al. 1994		-64.443000	-65.148000	547	290	13110	120	1230	120	3200	1970	11500	700	AIO	hbGM	
GC51	D172	Pudsey et al. 1994		-64.313000	-65.450000	575	210	12730	130	1230	120	1500	2770	13100	600	AIO	hbGM	
GC1702	TH96	Nishimura et al. 1999		-64.387146	-64.779050	522	195-198	14320	50	1230	120	2340	1110	13900	500	AIO	hbGM	
ODP-1098C	ODP Leg 178	Domack et al. 2001		-64.786142	-60.556385	1012	4192-4194	12250	60	1230	120	1260	30	12900	400	AIO	LDO	
PC-83	DF66	Harden et al. 1992		-64.671912	-62.996757	363	70-85	10240	250	1230	120	2760	1530	8400	1500	AIO	hbGM	

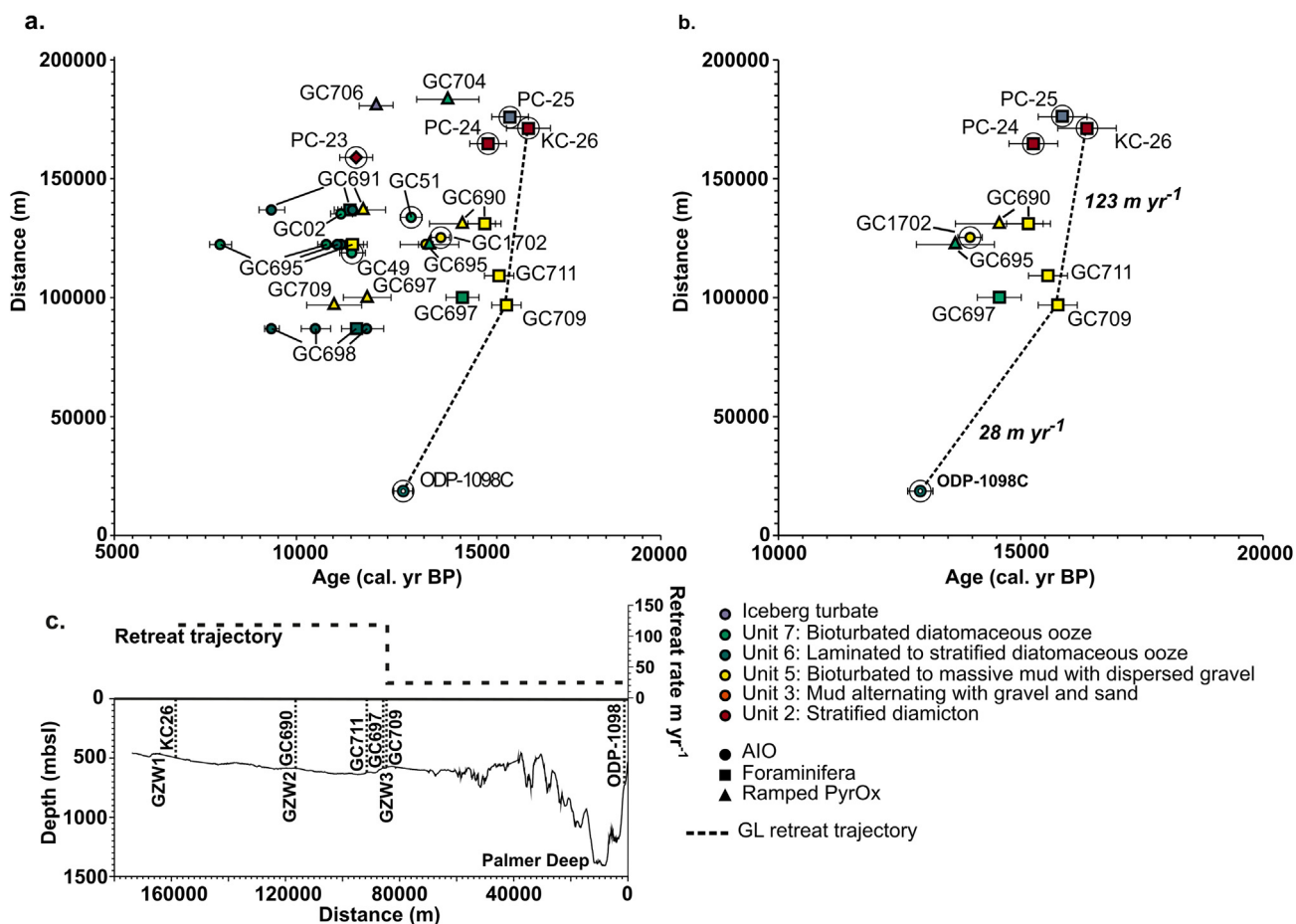


**Fig. 8.** (a) Calibrated AMS <sup>14</sup>C ages for JR284 and previously published cores versus distance along AHT. The positions of cores off the main trough axis were projected onto the centre line at the same latitude in order to calculate their distance along the trough. Colours of symbols indicate the different sediment types dated. (b) Reliable dates that constrain the timing of grounded ice retreat. (c) Calculated grounding-line retreat rates for the AHT palaeo-ice stream and bathymetric trough profile. This incorporates data from this study, Heroy and Anderson (2007; KC26) and Domack et al. (2001; ODP Site 1098). GZWs (1–3) are discussed in the text. (For interpretation of the references to colour in this figure legend, the reader is referred to the Web version of this article.)

shear strengths (up to 47 kPa) in some cores could indicate the presence of 'sticky-spots', although in most cases the downcore increase in shear strength likely reflects general compaction and dewatering processes (e.g., Halberstadt et al., 2018). As grounded ice began to retreat from its maximum position and prior to the establishment of seasonally open marine conditions, a complex and highly variable succession of 'transitional' sediments was deposited (Figs. 5 and 9; Units 2–5). Directly at the grounding line, sediment was likely derived from the seaward advection of the deformable sediments and rain out of basal debris in a confined sub-ice shelf cavity. This is observed as stratified diamictons (Unit 2) in cores GC704, GC702, GC695, GC709, GC697 (Fig. 5). Stratification was probably the result of a variable sediment flux as well as (tidal-) current activity, which would have modified grain sizes as detritus was settling through the water-column (i.e., before it was deposited) and after its deposition on the seabed by winnowing (Fig. 9a). Remobilisation of sea-floor sediments by grounding line oscillations (advance and retreat) and tidal pumping was probably also important in controlling the sedimentary signature (Drewry and Cooper, 1981; Powell et al., 1996; Ó Cofaigh et al., 2005; McKay et al., 2016). In cores GC702 and GC704 there is evidence of intermittent deposition of relatively coarse (Unit 2) and fine (Unit 5) sedimentary units. This could represent oscillations at a temporarily stable grounding line, where the depositional environment changes from grounding line proximal to a more distal position, or

the intermittent transport of unsorted sediment down the ocean-facing fronts of GZWs 1 and 2. The presence of Unit 3 in GC704 reflects strong current activity over the outer shelf, including winnowing.

A notable observation is that the thickness of transitional sediments (Units 2–5) imaged in the TOPAS profiles and found within the cores from AHT is highly variable. While it is not possible to resolve all lithological units within the TOPAS data, we can identify a moderate to high amplitude acoustic unit with continuous to discontinuous, interbedded reflectivity (e.g., Fig. 3; A2). Acoustic unit A2 is composed of units of laminated diatomaceous ooze (Unit 6) as well as transitional sediments. A2 appears thicker in bathymetric lows e.g., seawards of GZWs 2 and 3b (Fig. 3), and, therefore, the accumulation of sediments that comprise A2 could be the result of grounding line still stands. At other sites, such as GC692 and GC690, the transitional interval is virtually absent (Fig. 5). This indicates faster grounding line retreat over the outer shelf and between GZWs, providing insufficient time for the accumulation of thick transitional sediments. Focussing of transitional sediments in bathymetric lows is also likely to be an important factor, including at core site GC695, where we observe relatively thick transitional facies in the absence of a GZW.

Immediately downstream of the grounding line, melt/rain-out of debris from the ice shelf base will have continued to dominate sedimentation, depositing a wide-range of grain-sizes from mud to

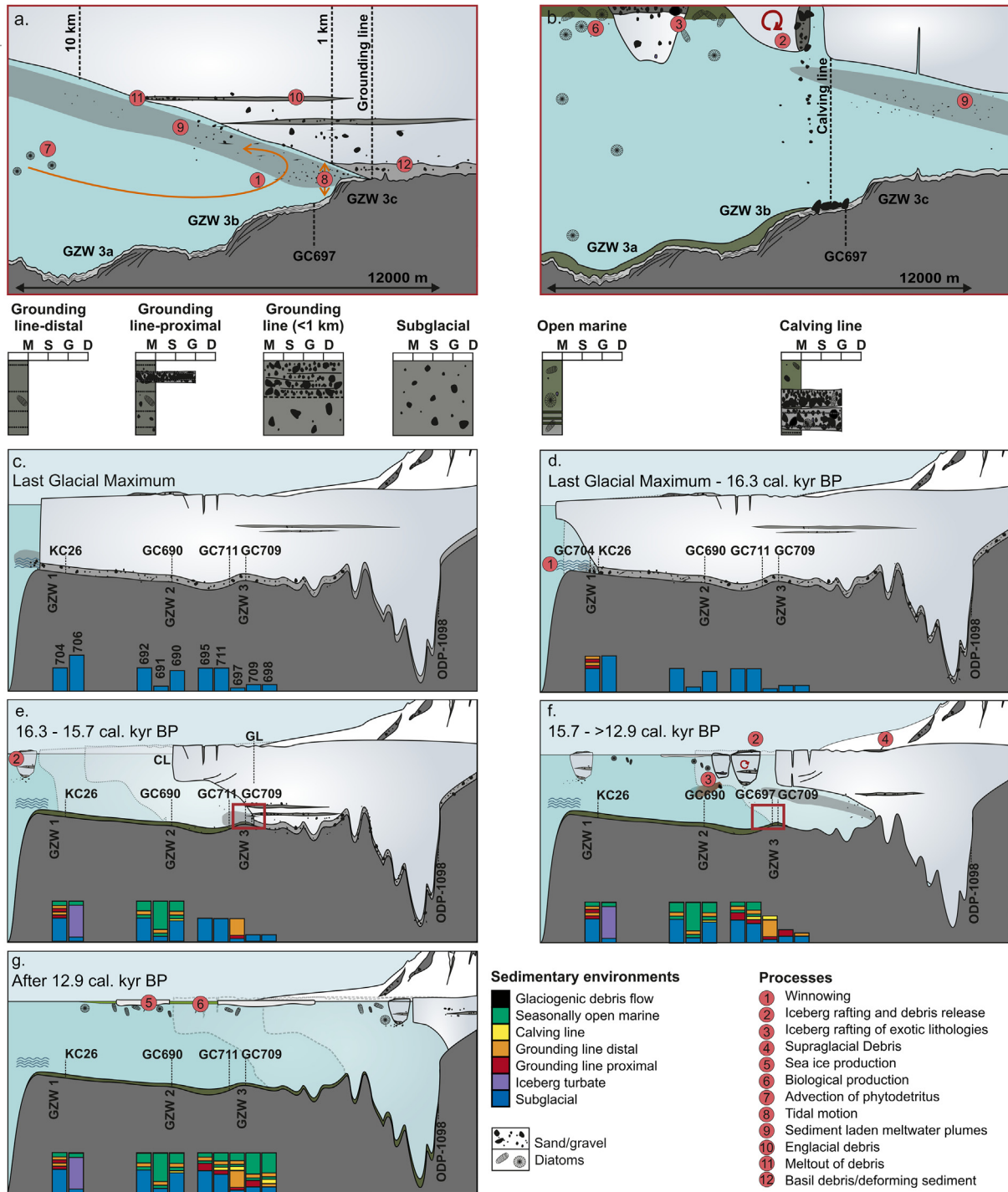


**Fig. 9.** (a–b) Schematic diagrams showing the depositional environments and processes at the ice stream grounding line (a) and calving line (b) at core site GC697 (M=mud, S=sand, G=gravel, D=diamict). (c–g) Schematic diagrams (not to scale) of grounding line retreat in AHT since the LGM (~23–19 cal kyr BP), including logs illustrating the deposition of lithological units observed in the JR284 sediment cores and their environmental settings. (c) Outer shelf grounding line position at the LGM. (d) Grounding line retreat from the outer shelf (core site KC26) at 16.3 cal kyr BP. (e) Grounding line retreat from core site KC26 at 16.3 cal kyr BP to core site GC709 at 15.7 cal kyr BP. The grounding line environment (red box) is shown in detail in Fig. 9a. (f) Grounding line retreat from core site GC709 at 15.7 cal kyr BP to a position seawards of Palmer Deep prior to 12.9 cal kyr BP, with the calving line assumed to be located at site GC697. The grounding line environment (red box) is shown in detail in Fig. 9b. (g) Grounding line position after 12.9 cal kyr BP. (For interpretation of the references to colour in this figure legend, the reader is referred to the Web version of this article.)

gravel, and in some cases larger cobbles and boulders (Units 2 and 3) (Drewry and Cooper, 1981; Powell, 1984; Powell et al., 1996; Domack and Harris, 1998; Smith et al., 2019) (Fig. 9a–b). As the grounding line continued to retreat, the coarser-grained proximal sediments are replaced by finer-grained plumes (Unit 4; GC697

and GC698) (Powell et al., 1996; Evans et al., 2005; Kilfeather et al., 2011; Witus et al., 2014; Smith et al., 2017) (Fig. 9). Deposition of these laminated sediments likely occurred beneath an ice shelf, as suggested by the low biogenic content (Domack and Williams, 1990; Powell et al., 1996; Smith et al., 2017). In core GC697, the

laminated muds are overlain by a sorted stratified diamicton that we attribute to deposition at the calving line (Fig. 9b). A similar stratigraphy is also seen in core GC698 (laminated muds overlain by stratified diamicton), although both units are thinner relative to GC697. The transition from sub-ice shelf to open-marine sedimentation represents the final phase of ice retreat in AHT and is characterised by the deposition of biogenic-rich muds with iceberg-rafted debris and diatomaceous oozes (Units 5 and 7) (Fig. 9b). In several cores (GC691, GC695, and GC698) a unit of laminated diatomaceous ooze occurs above the subglacial and grounding-line proximal sediments. It is interpreted to have been deposited during a period of extremely high productivity. Further investigations into the palaeo-productivity and palaeoceanographic changes in AHT following grounding line retreat are discussed in a companion paper (Roseby et al., in press).

The most prominent geomorphological features in AHT are the three well-developed GZWs. GZWs form during still-stands in grounding line retreat, with the volume of a wedge being controlled by sediment flux and the duration of the still stand (e.g., Alley et al., 1989, 2007; Larter and Vanneste, 1995; Dowdeswell and Fugelli, 2012; Dowdeswell et al., 2016; Bart et al., 2017). The formation of a GZW has usually been associated with the presence of an ice shelf (e.g., Larter and Vanneste, 1995; Dowdeswell and Fugelli, 2012; Smith et al., 2019), although this is not always the case (Simkins et al., 2018). With the exception of cores GC698 and GC697, which include sub-ice shelf sediments deposited distal from the grounding line, direct evidence for the existence of an extended ice shelf in AHT during post-LGM deglaciation is absent. The most expanded sequence of laminated mud/silt (Unit 4) occurs in GC697 and is 234 cm thick, indicating either high sediment supply or that GC697 was in a sub-ice shelf position for an extended period of time. The latter interpretation is compatible with the location of GC697, seaward of GZW 3c. AHT becomes constricted by shallow banks around Anvers and Hugo Islands, providing lateral pinning points which would favour ice shelf formation as well as providing shelter from wind, waves and currents (Fig. 2a) (Powell, 1984). The fact that comparably thick sub-ice shelf and calving line sediments were not recovered in other cores might suggest that (a) an extended ice shelf did not develop seawards of core site GC697, or (b) episodes of ice shelf cover were relatively short-lived and thus only characterised by coarse-grained, grounding line proximal facies (i.e., Units 2 and 3), (c) or that our understanding of the signature of ice shelf cover in the sedimentary record is incomplete (Smith et al., 2019).

## 5.2. Timing of grounded ice retreat in Anvers-Hugo Trough and regional comparisons

Grounded ice in AHT had extended to near the shelf edge at the LGM, and its subsequent retreat was punctuated by a series of still-stands documented by the presence of GZWs. Unfortunately, it was not possible to constrain the timing of APIS retreat from the shelf edge in AHT due to the lack of datable carbonate as well as complex sediment stratigraphy (gravelly sandy muds/iceberg turbate) in cores GC704 and GC706, respectively. Previously published foraminifera  $^{14}\text{C}$  ages from cores KC-26 and PC-24 (Fig. 8; Heroy and Anderson, 2005, 2007) indicate that grounded ice began its retreat sometime prior to ~16.3 cal kyr BP (Fig. 9c–d). The minimum time of grounded ice retreat across the mid-shelf is well constrained by dates from cores GC711 and GC709, indicating that glacial marine sedimentation on the middle shelf had begun by ~15.7 cal kyr BP (Figs. 8b and 9e). In Palmer Deep, AIO  $^{14}\text{C}$  ages from rhythmically interbedded diatomaceous ooze and pebbly mud directly overlying subglacial till at ODP Leg 178 Site 1098 indicate that grounded ice had retreated from the inner shelf by 12.9 cal kyr

BP (Figs. 8b and 9f–g) (Domack et al., 2001).

The overall pattern of deglaciation for AHT, with initial grounded ice retreat from the shelf edge sometime before 16.3 cal kyr BP and grounding-line retreat from the middle and inner-shelf areas by at least 15.7 cal kyr BP and 12.9 cal kyr BP, respectively, differs from previous studies (Pudsey et al., 1994; Heroy and Anderson, 2005, 2007). Specifically, the dates generated for this study suggest that the mid-shelf deglaciated earlier than in previous reconstructions (i.e., ~13.9 cal kyr BP at site GC-1702; Nishimura et al., 1999). Some earlier studies had suggested an even later deglaciation of the mid-shelf (e.g. PC-23: 11.6 cal kyr BP, Heroy and Anderson, 2005), which posed problems for an apparent 'early' deglaciation of Palmer Deep by 12.9 cal kyr BP (Domack et al., 2001). However, our new deglacial ages confirm an earlier retreat from the mid-shelf and help place recent retreat of the APIS in a longer-term context.

The revised timing of grounded ice retreat within AHT is largely consistent with the general deglaciation pattern of the WAP shelf (based on minimum age constraints on deglaciation; Fig. 10) and supports the idea of a north-south trend, whereby grounded ice retreated earlier in troughs in the NE than troughs in the SW (Heroy and Anderson, 2005; Livingstone et al., 2012; O Cofaigh et al., 2014).

## 5.3. Rate of grounded ice retreat in Anvers-Hugo Trough and regional comparisons

Based on our revised retreat chronology, calculated grounding line retreat rate across the outer and mid-shelf is  $123 \text{ m yr}^{-1}$ , slowing to  $28 \text{ m yr}^{-1}$  from the middle to inner shelf (Fig. 8c). However, given the low spatial resolution of dated cores, there could be considerable variability between sites. In comparison, 10% of marine-terminating APIS grounding lines retreated at rates faster than  $25 \text{ m yr}^{-1}$  between 2010 and 2016 (Konrad et al., 2018)

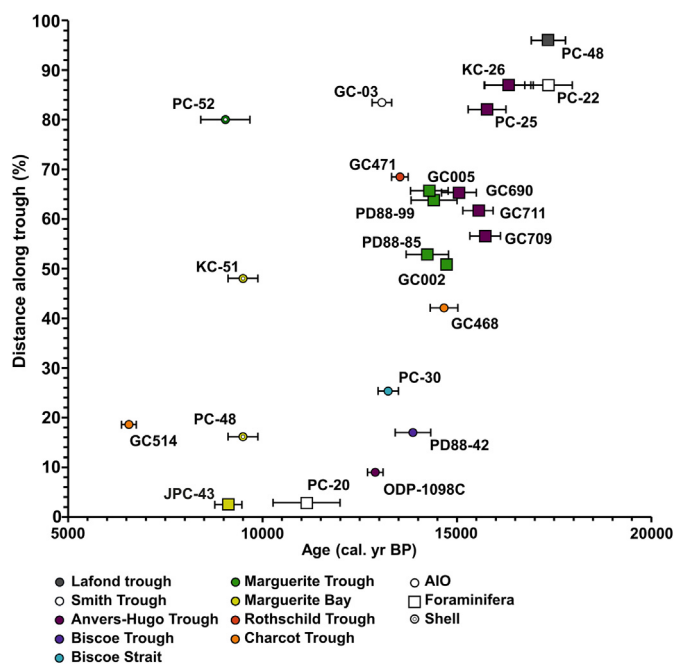


Fig. 10. Minimum ages for grounded ice retreat versus distance (normalised to % of trough length) along palaeo-ice stream troughs around the Antarctic Peninsula (see Fig. 1 for trough locations). The colours of symbols illustrate the location of each core site and their shape indicates the material dated (AIO, foraminifera or other calcareous shell). The included dates are from cores that have a reliable stratigraphy and lack age reversals (O Cofaigh et al., 2014). (For interpretation of the references to colour in this figure legend, the reader is referred to the Web version of this article.)

suggesting that post-LGM retreat rates on the outer shelf were considerably faster than current trends. We interpret the calculated retreat rates to reflect changes in bathymetry. AHT deepens from the outer to middle shelf and then shallows landward to a rougher seabed before deepening into Palmer Deep on the inner shelf (Fig. 8c; Fig. 2D in Livingstone et al., 2012). The rougher topography of the inner AHT shelf is likely to have resulted in greater basal drag just upstream of the grounding zone and provided more opportunities for the grounding line to pause on local pinning points (Larter et al., 2019). Furthermore, the topographic setting of the inner to middle shelf would have also resulted in highly convergent flow. Such convergent flow, which is documented by a pattern of streamlined bedforms (Larter et al., 2009), would slow down grounding line retreat (Fig. 2a) (Gudmundsson et al., 2012). Trough narrowing is also likely to have played a part in slowing down grounding line retreat by increasing lateral drag and promoting still-stands (Jamieson et al., 2012, 2014). In addition to a bathymetric control, we also note that Antarctic warming during the last glacial to interglacial transition was achieved by ~15 ka (Cuffey et al., 2016); this warming could have also been influential during the initial retreat of grounded ice over the outer and middle shelf by 15.7 cal kyr BP.

The cross-shelf profile of AHT resembles that of Belgica Trough into its Ronne Entrance tributary trough on the Bellingshausen Sea shelf, where an along-trough slow-down in grounding line retreat was also inferred (Hillenbrand et al., 2010b; Larter et al., 2014). Theory suggests that marine ice sheets that rest on a retrograde seabed are inherently unstable (i.e., MISI; Mercer, 1978; Schoof, 2007), and it appears that the landward sloping bed of the outer-mid shelf facilitated rapid grounding line retreat in AHT. Fast retreat rates in the outer-mid parts of Marguerite Trough (~80 m yr<sup>-1</sup> across a 140 km-long section of the outer trough) were also attributed to a reverse bed slope there (Jamieson et al., 2012). Comparable retreat rates following the LGM were calculated for Drygalski Basin, western Ross Sea, and Dotson-Getz Trough, western Amundsen Sea Embayment, where mean grounding line retreat occurred at a rate of 76 m yr<sup>-1</sup> (23–317 m yr<sup>-1</sup>) and 18–70 m yr<sup>-1</sup>, respectively (McKay et al., 2008; Smith et al., 2011; Livingstone et al., 2012). In contrast to AHT, grounding line retreat in Drygalski Basin and Dotson-Getz Trough was slower over the outer to middle shelf and accelerated towards the inner shelf. In Dotson-Getz Trough this increase in retreat rate is associated with a steepening of the reverse bed slope over the inner shelf (Graham et al., 2009; Smith et al., 2011).

While the presence of GZWs in AHT provides clear evidence that the grounding line paused on at least three occasions during its retreat, it has not been possible to accurately date individual wedge formation. The only firm conclusion is that GZW 2 and stacked GZW 3 on the mid-shelf must have been deposited over a period of ~600 years, between 16.3 cal kyr BP (date from core KC-26) to 15.7 cal kyr BP (date from core GC709). Whilst crude, the timing suggests that the wedges formed over hundreds rather than thousands of years and punctuated in a period of rapid grounding line retreat, similar to palaeo-ice stream retreat in Marguerite Trough (Jamieson et al., 2012, 2014). Deposition of GZW 2 and stacked GZW 3 within a period of ~600 years is consistent with estimates for the timing of GZW formation in the eastern Amundsen Sea Embayment based on sediment flux rates and GZW volume (potentially as little as 120 years, Graham et al., 2010; ≥600 years, Jakobsson et al., 2012), but contrasts with the stacked GZW in Whales Deep Basin, eastern Ross Sea, which formed over 3700 years (Bart et al., 2017). It should be noted that the Whales Deep

GZW is substantially larger (140 m thickness; ~543 km<sup>3</sup> volume) than those identified in this study (e.g., GZWs 1, 2 and stacked GZW 3 have heights, which approximate thickness, on the order of tens of metres), implying that the duration of grounding line still-stand may account for the difference in GZW size.

## 6. Conclusions

This study has used extensive new marine geological and geophysical data to reconstruct the glacial history of AHT, one of the largest palaeo-ice-stream troughs on the WAP shelf. Existing records indicate that the expanded APIS advanced to, or close to, the AHT continental shelf edge during the Last Glacial Maximum (23–19 cal kyr BP), with deglaciation of the outer shelf by ~16.3 cal kyr BP. Our new chronological data shows that grounded ice had retreated to the mid-shelf by ~15.7 cal kyr BP. During this 600-year interval, two GZWs (GZW 2 and 3) were deposited, suggesting that these landforms were formed over timescales of centuries rather than millennia.

Although based on limited age data, calculated retreat rates suggest that grounding line retreat in AHT was faster across the outer and middle shelf and slower towards the inner shelf. Such variability appears to have been driven by the bathymetry of AHT, and specifically the transition from a relatively smooth retrograde seafloor on the outer and middle shelf to relatively shallow, rugged bedrock on the inner shelf. Variations in the rate of grounding line retreat are also apparent in the distribution and thickness of sediments deposited between the time of grounding-line retreat and the onset of seasonal open-marine conditions. During fast ice stream retreat from the outer to middle shelf the main source for glacial debris was rapidly retreating, so there was insufficient time for thick deposits to accumulate. More generally, and in line with previous studies, we show that transitional deglacial sediments are highly spatially and temporally variable, not only in thickness but also sedimentological characteristics. This results from spatial variability in depositional processes, grounding line retreat rate, as well as sediment focussing into bathymetric lows. Finally, we conclude that the scarcity of calcareous micro-fossils continues to be a persistent problem for the radiocarbon dating of key environmental changes on this part of the Antarctic continental shelf. However, we also have shown that the use of a careful sampling strategy, which is guided by detailed sedimentological and multi-proxy information (e.g., Heroy and Anderson, 2005; Hillenbrand et al., 2010a,b, 2012; Smith et al., 2011, 2014), together with the application of different <sup>14</sup>C dating methods, which target different types of sediments and carbon-bearing material, provides reliable chronological frameworks for reconstructing Antarctic Ice Sheet retreat since the LGM. Further investigations into the palaeo-productivity and palaeoceanographic changes in AHT following grounding line retreat will be discussed in a companion paper (Roseby et al., in press).

## Author contributions

**Zoë A. Roseby:** Formal analysis, Investigation, Writing – original draft, Conceptualization, Visualization; **James A. Smith:** Writing – original draft, Conceptualization, Supervision; **Claus-Dieter Hillenbrand:** Writing – review & editing, Conceptualization, Supervision; **Matthieu J.B. Cartigny:** Writing – review & editing, Conceptualization, Supervision; **Brad E. Rosenheim:** Writing – review & editing, Methodology, Resources; **Kelly A. Hogan:** Writing – review & editing, Conceptualization, Visualization, Supervision;

**Claire S. Allen:** Writing – review & editing; **Amy Leventer:** Writing – review & editing; **Gerhard Kuhn:** Writing – review & editing, Methodology, Resources; **Werner Ehrmann:** Writing – review & editing, Methodology, Resources; **Robert D. Larter:** Writing – review & editing, Conceptualization, Supervision, Funding acquisition.

### Declaration of competing interest

The authors declare that they have no known competing financial interests or personal relationships that could have appeared to influence the work reported in this paper.

### Acknowledgments

This work was supported by the Natural Environment Research Council (grant number NE/L002531/1 and NE/J006548/1). Z. Roseby acknowledges further support from the International Association of Sedimentologists, Trans-Antarctic Association, British Sedimentological Research Group, Quaternary Research Association and the Alfred Wegener Institute, Helmholtz Centre for Polar and Marine Research (AWI). M. Cartigny was supported by a Collaborative Antarctic Science Scheme and a Research Fellowship from the Royal Society. This manuscript was additionally supported by the A4 project (Grant-Aid Agreement No. PBA/CC/18/01) funded under the Irish Marine Research Programme. We are grateful to the captains, officers, crew, support staff and scientists who participated in cruise JR284, as well as staff at the British Ocean Sediment Core Research Facility (BOSCORF, Southampton, UK) and Intertek NDT (Derby). We wish to thank and acknowledge M. Edwards, S. MacLachlan, D. Peck, C. Subt, R. Venturelli, L. Freeman, R. Fröhling-Teichert, B. J. Barrett, S. Wiebe and A. McNichol for their expert technical assistance and advice and Kathy Licht and Sara Benetti for their constructive reviews.

### Appendix A. Supplementary data

Supplementary data to this article can be found online at <https://doi.org/10.1016/j.quascirev.2022.107590>.

### References

- Alley, R.B., Blankenship, D.D., Rooney, S.T., Bentley, C.R., 1989. Sedimentation beneath ice shelves – the view from ice stream B. *Mar. Geol.* 85, 101–120.
- Alley, R.B., Anandakrishnan, S., Dupont, T.K., Parizek, B.R., Pollard, D., 2007. Effect of sedimentation on ice-sheet grounding-line stability. *Science* 315, 1838–1841.
- Anderson, J.B., 1999. *Antarctic Marine Geology*. Cambridge University Press, Cambridge.
- Anderson, J., 2005. Processed Multibeam Sonar Data (Version 2) Near the Antarctic Peninsula Acquired during Nathaniel B. Palmer Expedition NBP0201, 2002). Interdisciplinary Earth Data Alliance (IEDA).
- Andrews, J.T., Domack, E.W., Cunningham, W.L., Leventer, A., Licht, K.J., Jull, A.J.T., DeMaster, D.J., Jennings, A.E., 1999. Problems and possible solutions concerning radiocarbon dating of surface marine sediments, Ross Sea, Antarctica. *Quat. Res.* 52, 206–216.
- Annett, A.L., Skiba, M., Henley, S.F., Venables, H.J., Meredith, M.P., Statham, P.J., Ganeshram, R.S., 2015. Comparative roles of upwelling and glacial iron sources in Ryder Bay, coastal western Antarctic Peninsula. *Mar. Chem.* 176, 21–33.
- Annett, A.L., Fitzsimmons, J.N., Séguret, M.J.M., Lagerström, M., Meredith, M.P., Schofield, O., Sherrell, R.M., 2017. Controls on dissolved and particulate iron distributions in surface waters of the Western Antarctic Peninsula shelf. *Mar. Chem.* 196, 81–97.
- British Antarctic Survey, 1981a. British Antarctic Territory Geological Map, Sheet 3, BAS 500g Series, 1:500,000. British Antarctic Survey, Cambridge.
- British Antarctic Survey, 1981b. British Antarctic Territory Geological Map, Sheet 4, BAS 500g Series, 1:500,000. British Antarctic Survey, Cambridge.
- Arndt, J.E., Schenke, H.W., Jakobsson, M., Nitsche, F., Buys, G., Goleby, B., Rebesco, M., Bohoyo, F., Hong, J.K., Black, J., Greku, R., Udintsev, G., Barrios, F., Reynoso-Peralta, W., Morishita, T., Wigley, R., 2013. The International Bathymetric Chart of the Southern Ocean (IBCSO) Version 1.0 - a new bathymetric compilation covering circum-Antarctic waters. *Geophys. Res. Lett.* 40, 3111–3117.
- Arndt, J.E., Hillenbrand, C.-D., Grobe, H., Kuhn, G., Wacker, L., 2017. Evidence for a dynamic grounding-line in outer Filchner Trough, Antarctica, until the early Holocene. *Geology* 45, 1035–1038.
- Barker, P.F., Camerlenghi, A., 2002. Glacial history of the antarctic Peninsula from pacific margin sediments. In: Barker, P.F., Camerlenghi, A., Acton, G.D., Ramsay, A.T.S. (Eds.), *Antarctic Glacial History and Sea-Level Change*. Proceedings of the Ocean Drilling Program, vol. 178, pp. 1–40. Scientific Results.
- Bart, P.J., Krogmeier, B.J., Bart, M.P., Tulaczyk, S., 2017. The paradox of a long grounding during west antarctic ice sheet retreat in Ross Sea. *Sci. Rep.* 7, 1262.
- Bart, P.J., DeCesare, M., Rosenheim, B.E., Majewski, W., McGlannan, A., 2018. A centuries-long delay between a paleo-ice-shelf collapse and grounding-line retreat in the Whales Deep Basin, eastern Ross Sea, Antarctica. *Sci. Rep.* 8, 12392.
- Batchelor, C.L., Dowdeswell, J.A., 2015. Ice-sheet grounding-zone wedges (GZWs) on high-latitude continental margins. *Mar. Geol.* 363, 65–92.
- Bracegirdle, T.J., Colleoni, F., Abram, N.J., Bertler, N.A.N., Dixon, D.A., England, M., Favier, V., Fogwill, C.J., Fyfe, J.C., Goodwin, I., Goosse, H., Hobbs, W., Jones, J.M., Keller, E.D., Khan, A.L., Phipps, S.J., Raphael, M.N., Russell, J., Sime, L., Thomas, E.R., van den Broeke, M.R., Wainer, I., 2019. Back to the future: using long-term observational and paleo-proxy reconstructions to improve model projections of antarctic climate. *Geosciences* 9, 255.
- Brachfeld, S., Domack, E., Kissel, C., Laj, C., Leventer, A., Ishman, S., Gilbert, R., Camerlenghi, A., Eglinton, L.B., 2003. Holocene history of the Larsen-A Ice Shelf constrained by geomagnetic paleointensity dating. *Geology* 31, 749–752.
- Briggs, R.D., Tarasov, L., 2013. How to evaluate model-derived deglaciation chronologies: a case study using Antarctica. *Quat. Sci. Rev.* 63, 109–127.
- Caress, D.W., Chayes, D.N., 1996. Improved processing of hydrosweep DS multibeam data on the R/V maurice ewing. *Mar. Geophys. Res.* 18, 631–650.
- Caress, D.W., Chayes, D.N., dos Santos Ferreira, C., 2018. MB-system: Mapping the Seafloor available at: <https://www.mbari.org/products/research-software/mb-system>. (Accessed December 2018). accessed.
- Clark, C.D., 1993. Mega-scale glacial lineations and cross-cutting ice-flow landforms. *Earth Surf. Process. Landforms* 18, 1–29.
- Cook, A.J., Vaughan, D.G., 2010. Overview of areal changes of the ice shelves on the Antarctic Peninsula over the past 50 years. *Cryosphere* 4, 77–98.
- Cook, A.J., Holland, P.R., Meredith, M.P., Murray, T., Luckman, A., Vaughan, D.G., 2016. Oceanic forcing of glacier retreat in the western Antarctic Peninsula. *Science* 353, 283–286.
- Crosta, X., Sturm, A., Armand, L., Pichon, J.-J., 2004. Late Quaternary sea ice history in the Indian sector of the Southern Ocean as recorded by diatom assemblages. *Mar. Micropaleontol.* 50, 209–223.
- Crosta, X., Debret, M., Denis, D., Courty, M.A., Ther, O., 2007. Holocene long- and short-term climate changes off Adélie Land, East Antarctica. *C- cubed* 8.
- Cuffey, K.M., Clow, G.D., Steig, E.J., Buizert, C., Fudge, T.J., Koutnik, M., Waddington, E.D., Alley, R.B., Severinghaus, J.P., 2016. Deglacial temperature history of West Antarctica. *Proc. Natl. Acad. Sci. Unit. States Am.* 113, 14249–14254.
- DeConto, R.M., Pollard, D., 2016. Contribution of Antarctica to past and future sea-level rise. *Nature* 531, 591.
- Domack, E.W., 1992. Modern carbon-14 ages and reservoir corrections for the Antarctic Peninsula and Gerlache Strait area. *Antarct. J. U. S.* 27, 63–64.
- Domack, E., 2001. Processed Multibeam Sonar Data (Version 2) Near the Antarctic Peninsula Acquired during Nathaniel B. Palmer Expedition NBP0107. Interdisciplinary Earth Data Alliance (IEDA), 2005.
- Domack, E.W., Harris, P.T., 1998. A new depositional model for ice shelves, based upon sediment cores from the Ross Sea and the Mac. Robertson shelf, Antarctica. *Ann. Glaciol.* 27, 281–284.
- Domack, E.W., Powell, R., 2018. Chapter 7 - modern glaciomarine environments and sediments: an antarctic perspective. In: Menzies, J., van der Meer, J.J.M. (Eds.), *Past Glacial Environments*, second ed. Elsevier, pp. 181–272.
- Domack, E.W., Williams, C.R., 1990. Fine structure and suspended sediment transport in three antarctic fjords, contributions to antarctic Research I. *American Geophysical Union* 50, 71–89.
- Domack, E., O'Brien, P., Harris, P., Santis, L., Raker, B., 1998. Late Quaternary sediment facies in Prydz Bay, East Antarctica and their relationship to glacial advance onto the continental shelf. *Antarct. Sci.* 10, 236–246.
- Domack, E.W., Jacobson, E.A., Shipp, S., Anderson, J.B., 1999. Late pleistocene–holocene retreat of the west antarctic ice-sheet system in the Ross Sea: Part 2—sedimentological and stratigraphic signature. *Geol. Soc. Am. Bull.* 111, 1517–1536.
- Domack, E., Leventer, A., Dunbar, R., Taylor, F., Brachfeld, S., Sjunneskog, C., 2001. Chronology of the palmer deep site, antarctic Peninsula: a Holocene palaeoenvironmental reference for the circum-antarctic. *Holocene* 11, 1–9.
- Domack, E., Duran, D., Leventer, A., Ishman, S., Doane, S., McCallum, S., Amblas, D., Ring, J., Gilbert, R., Prentice, M., 2005. Stability of the larsen B ice shelf on the antarctic Peninsula during the Holocene epoch. *Nature* 436, 681–685.
- Domack, E., Amblàs, D., Gilbert, R., Brachfeld, S., Camerlenghi, A., Rebesco, M., Canals, M., Urgeles, R., 2006. Subglacial morphology and glacial evolution of the Palmer deep outlet system, Antarctic Peninsula. *Geomorphology* 75, 125–142.
- Dowdeswell, J.A., Fugelli, E.M.G., 2012. The Seismic Architecture and Geometry of Grounding-Zone Wedges Formed at the Marine Margins of Past Ice Sheets. *Geological Society of America Bulletin*.
- Dowdeswell, J.A., Ó Cofaigh, C., Pudsey, C.J., 2004. Thickness and extent of the subglacial till layer beneath an Antarctic paleo-ice stream. *Geology* 32, 13–16.
- Dowdeswell, J.A., Ottesen, D., Evans, J., Ó Cofaigh, C., Anderson, J.B., 2008. Submarine glacial landforms and rates of ice-stream collapse. *Geology* 36, 819–822.

- Dowdeswell, J.A., Ottesen, D., Forwick, M., 2016. Grounding-zone wedges on the western Svalbard shelf. *Geological Society, London, Memoirs* 46, 233–234.
- Drewry, D.J., Cooper, A.P.R., 1981. Processes and models of antarctic glaciomarine sedimentation. *Ann. Glaciol.* 2, 117–122.
- Ehrmann, W.U., Melles, M., Kuhn, G., Grobe, H., 1992. Significance of clay mineral assemblages in the Antarctic Ocean. *Mar. Geol.* 107, 249–273.
- Ehrmann, W., Hillenbrand, C.-D., Smith, J.A., Graham, A.G.C., Kuhn, G., Larter, R.D., 2011. Provenance changes between recent and glacial-time sediments in the Amundsen Sea embayment, West Antarctica: clay mineral assemblage evidence. *Antarct. Sci.* 23, 471–486.
- Evans, J., Pudsey, C.J., 2002. Sedimentation associated with Antarctic Peninsula ice shelves: implications for palaeoenvironmental reconstructions of glaciomarine sediments. *J. Geol. Soc.* 159, 233–237.
- Evans, J., Pudsey, C.J., Ó Cofaigh, C., Morris, P., Domack, E., 2005. Late Quaternary glacial history, flow dynamics and sedimentation along the eastern margin of the Antarctic Peninsula Ice Sheet. *Quat. Sci. Rev.* 24, 741–774.
- Favier, L., Durand, G., Cornford, S.L., Gudmundsson, G.H., Gagliardini, O., Gillet-Chaulet, F., Zwinger, T., Payne, A.J., Le Brocq, A.M., 2014. Retreat of Pine Island Glacier controlled by marine ice-sheet instability. *Nat. Clim. Change* 4, 117.
- Garibotti, I., Vernet, M., Ferrario, M., Smith, R., Ross, R., Quetin, L.B., 2003. Phytoplankton spatial distribution patterns along the western Antarctic Peninsula (southern ocean). *Marine Ecology-progress Series - MAR ECOL-PROGR SER* 261, 21–39.
- Graham, A.G.C., Larter, R.D., Gohl, K., Hillenbrand, C.-D., Smith, J.A., Kuhn, G., 2009. Bedform signature of a West Antarctic palaeo-ice stream reveals a multi-temporal record of flow and substrate control. *Quat. Sci. Rev.* 28, 2774–2793.
- Graham, A.G.C., Larter, R.D., Gohl, K., Dowdeswell, J.A., Hillenbrand, C.D., Smith, J.A., Evans, J., Kuhn, G., Deen, T., 2010. Flow and retreat of the late quaternary pine island-thwaites palaeo-ice stream, west Antarctica. *J. Geophys. Res.: Earth Surf.* 115.
- Greenwood, S.L., Simkins, L.M., Winsborrow, M.C.M., Bjarnadóttir, L.R., 2021. Exceptions to bed-controlled ice sheet flow and retreat from glaciated continental margins worldwide. *Sci. Adv.* 7.
- Gudmundsson, G.H., Krug, J., Durand, G., Favier, L., Gagliardini, O., 2012. The stability of grounding lines on retrograde slopes. *Cryosphere* 6, 1497–1505.
- Halberstadt, A.R.W., Simkins, L.M., Anderson, J.B., Prothro, L.O., Bart, P.J., 2018. Characteristics of the deforming bed: till properties on the deglaciated Antarctic continental shelf. *J. Glaciol.* 64, 1014–1027.
- Harden, S.L., DeMaster, D.J., Nittrouer, C.A., 1992. Developing sediment geochronologies for high-latitude continental shelf deposits: a radiochemical approach. *Mar. Geol.* 103, 69–97.
- Heaton, T.J., Köhler, M., Butzin, M., Bard, E., Reimer, R.W., Austin, W.E.N., Bronk Ramsey, C., Grootes, P.M., Hughen, K.A., Kromer, B., Reimer, P.J., Adkins, J., Burke, A., Cook, M.S., Olsen, J., Skinner, L.C., 2020. Marine20—the marine radiocarbon age calibration curve (0–55,000 cal BP). *Radiocarbon* 62, 779–820.
- Hemer, M.A., Harris, P.T., 2003. Sediment core from beneath the Amery Ice Shelf, East Antarctica, suggests mid-Holocene ice-shelf retreat. *Geology* 31, 127–130.
- Hemer, M.A., Post, A.L., O'Brien, P.E., Craven, M., Truswell, E.M., Roberts, D., Harris, P.T., 2007. Sedimentological signatures of the sub-Amery Ice Shelf circulation. *Antarct. Sci.* 19, 497–506.
- Heroy, D.C., Anderson, J.B., 2005. Ice-sheet extent of the antarctic Peninsula region during the last glacial maximum (LGM)—insights from glacial geomorphology. *Geol. Soc. Am. Bull.* 117, 1497–1512.
- Heroy, D.C., Anderson, J.B., 2007. Radiocarbon constraints on antarctic Peninsula ice sheet retreat following the last glacial maximum (LGM). *Quat. Sci. Rev.* 26, 3286–3297.
- Hillenbrand, C.-D., Ehrmann, W., 2001. Distribution of clay minerals in drift sediments on the continental rise west of the Antarctic Peninsula, ODP Leg 178, Sites 1095 and 1096. In: Barker, P.F., Camerlenghi, A., Acton, G.D., Ramsay, A.T.S. (Eds.), *Proc. ODP, Sci. Results*, p. 178.
- Hillenbrand, C.-D., Grobe, H., Diekmann, B., Kuhn, G., Fütterer, D.K., 2003. Distribution of clay minerals and proxies for productivity in surface sediments of the Bellingshausen and Amundsen seas (West Antarctica) – relation to modern environmental conditions. *Mar. Geol.* 193, 253–271.
- Hillenbrand, C.-D., Baesler, A., Grobe, H., 2005. The sedimentary record of the last glaciation in the western Bellingshausen Sea (West Antarctica): implications for the interpretation of diamictos in a polar-marine setting. *Mar. Geol.* 216, 191–204.
- Hillenbrand, C.-D., Ehrmann, W., Larter, R.D., Benetti, S., Dowdeswell, J.A., Ó Cofaigh, C., Graham, A.G.C., Grobe, H., 2009. Clay mineral provenance of sediments in the southern Bellingshausen Sea reveals drainage changes of the west antarctic ice sheet during the late quaternary. *Mar. Geol.* 265, 1–18.
- Hillenbrand, C.-D., Smith, J.A., Kuhn, G., Esper, O., Gersonde, R., Larter, R.D., Maher, B., Moreton, S.G., Shimmield, T.M., Korte, M., 2010a. Age assignment of a diatomaceous ooze deposited in the western Amundsen Sea embayment after the last glacial maximum. *J. Quat. Sci.* 25, 280–295.
- Hillenbrand, C.-D., Larter, R.D., Dowdeswell, J.A., Ehrmann, W., Ó Cofaigh, C., Benetti, S., Graham, A.G.C., Grobe, H., 2010b. The sedimentary legacy of a palaeo-ice stream on the shelf of the southern Bellingshausen Sea: clues to West Antarctic glacial history during the Late Quaternary. *Quat. Sci. Rev.* 29, 2741–2763.
- Hillenbrand, C.-D., Melles, M., Kuhn, G., Larter, R.D., 2012. Marine. Geological constraints for the grounding-line position of the antarctic ice sheet on the southern weddell Sea shelf at the last glacial maximum. *Quat. Sci. Rev.* 32, 25–47.
- Jacobs, S.S., Jenkins, A., Giulivi, C.F., Dutrieux, P., 2011. Stronger ocean circulation and increased melting under Pine Island Glacier ice shelf. *Nat. Geosci.* 4, 519–523.
- Jakobsson, M., Anderson, J.B., Nitsche, F.O., Gyllencreutz, R., Kirshner, A.E., Kirchner, N., O'Regan, M., Mohammad, R., Eriksson, B., 2012. Ice sheet retreat dynamics inferred from glacial morphology of the central Pine Island Bay Trough, West Antarctica. *Quat. Sci. Rev.* 38, 1–10.
- Jamieson, S.S.R., Vieli, A., Livingstone, S.J., Ó Cofaigh, C., Stokes, C., Hillenbrand, C.-D., Dowdeswell, J.A., 2012. Ice-stream stability on a reverse bed slope. *Nat. Geosci.* 5, 799–802.
- Jamieson, S.S.R., Vieli, A., Ó Cofaigh, C., Stokes, C.R., Livingstone, S.J., Hillenbrand, C.-D., 2014. Understanding controls on rapid ice-stream retreat during the last deglaciation of Marguerite Bay, Antarctica, using a numerical model. *J. Geophys. Res.: Earth Surf.* 119, 247–263.
- Joughin, I., Smith, B.E., Medley, B., 2014. Marine ice sheet collapse potentially under way for the thwaites glacier basin, west Antarctica. *Science* 344, 735–738.
- Kilfeather, A.A., Ó Cofaigh, C., Lloyd, J.M., Dowdeswell, J.A., Xu, S., Moreton, S.G., 2011. Ice-stream retreat and ice-shelf history in Marguerite Trough, antarctic Peninsula: sedimentological and foraminiferal signatures. *Geol. Soc. Am. Bull.* 123, 997–1015.
- King, L.H., 1993. Till in the marine environment. *J. Quat. Sci.* 8, 347–358.
- King, M.A., Bingham, R.J., Moore, P., Whitehouse, P.L., Bentley, M.J., Milne, G.A., 2012. Lower satellite-gravimetry estimates of Antarctic sea-level contribution. *Nature* 491, 586–589.
- Kirkham, J.D., Hogan, K.A., Larter, R.D., Arnold, N.S., Nitsche, F.O., Gollledge, N.R., Dowdeswell, J.A., 2019. Past water flow beneath pine Island and thwaites glaciers, west Antarctica. *Cryosphere* 13, 1959–1981.
- Konrad, H., Shepherd, A., Gilbert, L., Hogg, A.E., McMillan, M., Muir, A., Slater, T., 2018. Net retreat of Antarctic glacier grounding lines. *Nat. Geosci.* 11, 258–262.
- Larter, R.D., Barker, P.F., 1989. Seismic stratigraphy of the Antarctic Peninsula Pacific margin: a record of Pliocene-Pleistocene ice volume and paleoclimate. *Geology* 17, 731–734.
- Larter, R.D., Vanneste, L.E., 1995. Relict subglacial deltas on the Antarctic Peninsula outer shelf. *Geology* 23, 33–36.
- Larter, R.D., Rebesco, M., Vanneste, L.E., Gambôa, L.A.P., Barker, P.F., 1997. Cenozoic tectonic, sedimentary and glacial history of the continental shelf west of Graham Land, Antarctic Peninsula. In: Barker, P.F., Cooper, A.K. (Eds.), *Geology and Seismic Stratigraphy of the Antarctic Margin*, 2, vol. 71. American Geophysical Union, Washington DC, Antarctic Research Series, pp. 1–27.
- Larter, R.D., Graham, A.G.C., Gohl, K., Kuhn, G., Hillenbrand, C.-D., Smith, J.A., Deen, T.J., Livermore, R.A., Schenke, H.-W., 2009. Subglacial bedforms reveal complex basal regime in a zone of paleo-ice stream convergence, Amundsen Sea embayment, West Antarctica. *Geology* 37, 411–414.
- Larter, R.D., Anderson, J.B., Graham, A.G.C., Gohl, K., Hillenbrand, C.-D., Jakobsson, M., Johnson, J.S., Kuhn, G., Nitsche, F.O., Smith, J.A., Witus, A.E., Bentley, M.J., Dowdeswell, J.A., Ehrmann, W., Klages, J.P., Lindow, J., Ó Cofaigh, C., Spiegel, C., 2014. Reconstruction of changes in the Amundsen Sea and Bellingshausen Sea sector of the west antarctic ice sheet since the last glacial maximum. *Quat. Sci. Rev.* 100, 55–86.
- Larter, R.D., Hogan, K.A., Hillenbrand, C.-D., Smith, J.A., Batchelor, C.L., Cartigny, M., Tate, A.J., Kirkham, J.D., Roseby, Z.A., Kuhn, G., Graham, A.G.C., Dowdeswell, J.A., 2019. Subglacial hydrological control on flow of an Antarctic Peninsula palaeo-ice stream. *Cryosphere* 13, 1583–1596.
- Lavoie, C., Domack, E.W., Pettit, E.C., Scambos, T.A., Larter, R.D., Schenke, H.W., Yoo, K.C., Gutt, J., Wellner, J., Canals, M., Anderson, J.B., Amblas, D., 2015. Configuration of the northern antarctic Peninsula ice sheet at LGM based on a new synthesis of seabed imagery. *Cryosphere* 9, 613–629.
- Lepp, A.P., Simkins, L.M., Anderson, J.B., Clark, R.W., Wellner, J.S., Hillenbrand, C.-D., Smith, J.A., Lehrmann, A.A., Totten, R., Larter, R.D., Hogan, K.A., Nitsche, F.O., Graham, A.G.C., Wacker, L., 2022. Sedimentary Signatures of Persistent Subglacial Meltwater Drainage From Thwaites Glacier, Antarctica. *Frontiers in Earth Science* 10.
- Leventer, A., Domack, E., A Dunbar, R., A Pike, J., Stickley, C., Maddison, E., Brachfeld, S., Manley, P., McClennen, C., 2006. Marine sediment record from the East Antarctic margin reveals dynamics of ice sheet recession. *GSA Today (Geol. Soc. Am.)* 16, 4–10.
- Leventer, A., Domack, E., Barkoukis, A., McAndrews, B., Murray, J., 2002. Laminations from the palmer deep: a diatom-based interpretation. *Paleoceanography* 17.
- Licht, K.J., Jennings, A.E., Andrews, J.T., Williams, K.M., 1996. Chronology of late Wisconsin ice retreat from the western Ross Sea, Antarctica. *Geology* 24, 223–226.
- Licht, K.J., Cunningham, W.L., Andrews, J.T., Domack, E.W., Jennings, A.E., 1998. Establishing chronologies from acid-insoluble organic 14C dates on antarctic (Ross Sea) and arctic (north atlantic) marine sediments. *Polar Res.* 17, 203–216.
- Licht, K.J., Dunbar, N.W., Andrews, J.T., Jennings, A.E., 1999. Distinguishing subglacial till and glacial marine diamictos in the western Ross Sea, Antarctica: implications for a last glacial maximum grounding line. *Geol. Soc. Am. Bull.* 111, 91–103.
- Livingstone, S.J., Ó Cofaigh, C., Stokes, C.R., Hillenbrand, C.-D., Vieli, A., Jamieson, S.S.R., 2012. Antarctic palaeo-ice streams. *Earth Sci. Rev.* 111, 90–128.
- Livingstone, S.J., Stokes, C.R., Ó Cofaigh, C., Hillenbrand, C.-D., Vieli, A., Jamieson, S.S.R., Spagnolo, M., Dowdeswell, J.A., 2016. Subglacial processes on an Antarctic ice stream bed. 1: sediment transport and bedform genesis inferred from marine geophysical data. *J. Glaciol.* 62, 270–284.
- Maddison, E.J., Pike, J., Leventer, A., Domack, E.W., 2005. Deglacial seasonal and sub-seasonal diatom record from Palmer Deep, Antarctica. *J. Quat. Sci.* 20, 435–446.

- Maddison, E.J., Pike, J., Leventer, A., Dunbar, R., Brachfeld, S., Domack, E.W., Manley, P., McClennen, C., 2006. Post-glacial seasonal diatom record of the mertz glacier polynya, east Antarctica. *Mar. Micropaleontol.* 60, 66–88.
- McKay, R.M., Dunbar, G.B., Naish, T.R., Barrett, P.J., Carter, L., Harper, M., 2008. Retreat history of the Ross ice sheet (shelf) since the last glacial maximum from deep-basin sediment cores around Ross Island. *Palaeogeogr. Palaeoclimatol. Palaeoecol.* 260, 245–261.
- McKay, R., Golledge, N.R., Maas, S., Naish, T., Levy, R., Dunbar, G., Kuhn, G., 2016. Antarctic marine ice-sheet retreat in the Ross Sea during the early Holocene. *Geology* 44, 7–10.
- Mercer, J.H., 1978. West Antarctic ice sheet and CO<sub>2</sub> greenhouse effect: a threat of disaster. *Nature* 271, 321–325.
- Minzoni, R.T., Majewski, W., Anderson, J.B., Yokoyama, Y., Fernandez, R., Jakobsson, M., 2017. Oceanographic influences on the stability of the cosgrove ice shelf, Antarctica. *Holocene* 27, 1645–1658.
- Müller, P.J., Schneider, R., 1993. An automated leaching method for the determination of opal in sediments and particulate matter. *Deep Sea Res. Oceanogr. Res. Pap.* 40, 425–444.
- Neuhaus, S.U., Tulaczyk, S.M., Stansell, N.D., Coenen, J.J., Scherer, R.P., Mikucki, J.A., Powell, R.D., 2021. Did Holocene climate changes drive West Antarctic grounding line retreat and readvance? *The Cryosphere* 15, 4655–4673.
- Nishimura, A., Tanahashi, M., Tokuhashi, S., Oda, H., Nakasone, T., 1999. Marine sediment cores from the continental shelf around Anvers Island, Antarctic Peninsula region. *Polar Geosci.* 12, 215–226.
- Ó Cofaigh, C., Pudsey, C.J., Dowdeswell, J.A., Morris, P., 2002. Evolution of subglacial bedforms along a paleo-ice stream, Antarctic Peninsula continental shelf. *Geophys. Res. Lett.* 29, 41–44.
- Ó Cofaigh, C., Dowdeswell, J.A., Allen, C.S., Hiemstra, J.F., Pudsey, C.J., Evans, J., Evans, D.J.A., 2005. Flow dynamics and till genesis associated with a marine-based Antarctic palaeo-ice stream. *Quat. Sci. Rev.* 24, 709–740.
- Ó Cofaigh, C., Evans, J., Dowdeswell, J.A., Larter, R.D., 2007. Till characteristics, genesis and transport beneath Antarctic paleo-ice streams. *J. Geophys. Res.: Earth Surf.* 112.
- Ó Cofaigh, C., Davies, B.J., Livingstone, S.J., Smith, J.A., Johnson, J.S., Hocking, E.P., Hodgson, D.A., Anderson, J.B., Bentley, M.J., Canals, M., Domack, E., Dowdeswell, J.A., Evans, J., Glasser, N.F., Hillenbrand, C.-D., Larter, R.D., Roberts, S.J., Simms, A.R., 2014. Reconstruction of ice-sheet changes in the antarctic Peninsula since the last glacial maximum. *Quat. Sci. Rev.* 100, 87–110.
- Ohkouchi, N., Eglinton, T.I., Hayes, J.M., 2003. Radiocarbon dating of individual fatty acids as a tool for refining antarctic margin sediment chronologies. *Radiocarbon* 45, 17–24.
- Ottesen, D., Stokes, C.R., Rise, L., Olsen, L., 2008. Ice-sheet dynamics and ice streaming along the coastal parts of northern Norway. *Quat. Sci. Rev.* 27, 922–940.
- Paolo, F.S., Fricker, H.A., Padman, L., 2015. Volume loss from Antarctic ice shelves is accelerating. *Science* 348, 327–331.
- Pike, J., Allen, C.S., Leventer, A., Stickley, C.E., Pudsey, C.J., 2008. Comparison of contemporary and fossil diatom assemblages from the western Antarctic Peninsula shelf. *Mar. Micropaleontol.* 67, 274–287.
- Pirring, M., Fütterer, D., Grobe, H., Matthiessen, J., Niessen, F., 2002. Magnetic susceptibility and ice-rafted debris in surface sediments of the Nordic Seas: implications for Isotope Stage 3 oscillations. *Geo Mar. Lett.* 22, 1–11.
- Pollard, D., DeConto, R.M., Alley, R.B., 2015. Potential Antarctic Ice Sheet retreat driven by hydrofracturing and ice cliff failure. *Earth Planet Sci. Lett.* 412, 112–121.
- Post, A.L., Galton-Fenzi, B.K., Riddle, M.J., Herraiz-Borreguero, L., O'Brien, P.E., Hemer, M.A., McMinn, A., Rasch, D., Craven, M., 2014. Modern sedimentation, circulation and life beneath the amery ice shelf, east Antarctica. *Continent. Shelf Res.* 74, 77–87.
- Powell, R.D., 1984. Glacimarine processes and inductive lithofacies modelling of ice shelf and tidewater glacier sediments based on Quaternary examples. *Mar. Geol.* 57, 1–52.
- Powell, R.D., Dawber, M., McInnes, J.N., Pyne, A.R., 1996. Observations of the grounding-line area at a floating glacier terminus. *Ann. Glaciol.* 22, 217–223.
- Prothro O, Lindsay, Simkins M, Lauren, Majewski, Wojciech, Anderson B, John, 2018. Glacial retreat patterns and processes determined from integrated sedimentology and geomorphology records. *Marine Geology* 395, 104–119.
- Pudsey, C.J., 2000. Sedimentation on the continental rise west of the Antarctic Peninsula over the last three glacial cycles. *Mar. Geol.* 167, 313–338.
- Pudsey, C.J., 2002. Neogene record of Antarctic Peninsula glaciation in continental rise sediments: ODP Leg 178, Site 1095. In: Barker, P.F., Camerlenghi, A., Acton, G.D., Ramsay, A.T.S. (Eds.), *Proceedings of the Ocean Drilling Program Scientific Results*, vol. 178. Ocean Drilling Program, Texas A&M University, College Station, TX, pp. 1–25.
- Pudsey, C.J., Barker, P.F., Larter, R.D., 1994. Ice sheet retreat from the Antarctic Peninsula shelf. *Continent. Shelf Res.* 14, 1647–1675.
- Pudsey, C.J., Murray, J.W., Appleby, P., Evans, J., 2006. Ice shelf history from petrographic and foraminiferal evidence, Northeast Antarctic Peninsula. *Quat. Sci. Rev.* 25, 2357–2379.
- Rebesco, M., Camerlenghi, A., De Santis, L., Domack, E., Kirby, M., 1998. Seismic stratigraphy of Palmer Deep: a fault-bounded late Quaternary sediment trap on the inner continental shelf, Antarctic Peninsula Pacific margin. *Mar. Geol.* 151, 89–110.
- Reinardy, B.T.I., Hiemstra, J.F., Murray, T., Hillenbrand, C.-D., Larter, R.D., 2011a. Till genesis at the bed of an Antarctic Peninsula palaeo-ice stream as indicated by micromorphological analysis. *Boreas* 40, 498–517.
- Reinardy, B.T.I., Larter, R.D., Hillenbrand, C.-D., Murray, T., Hiemstra, J.F., Booth, A.D., 2011b. Streaming flow of an Antarctic Peninsula palaeo-ice stream, both by basal sliding and deformation of substrate. *J. Glaciol.* 57, 596–608.
- Rignot, E., Mougnot, J., Morlighem, M., Seroussi, H., Scheuchl, B., 2014. Widespread, rapid grounding line retreat of Pine Island, Thwaites, Smith, and Kohler glaciers, west Antarctica, from 1992 to 2011. *Geophys. Res. Lett.* 41, 3502–3509.
- Rignot, E., Mougnot, J., Scheuchl, B., van den Broeke, M., van Wessem, M.J., Morlighem, M., 2019. Four decades of antarctic ice sheet mass balance from 1979–2017. *Proc. Natl. Acad. Sci. Unit. States Am.* 116, 1095.
- Roseby, A.Z., Smith, J.A., Hillenbrand, C.-D., Allen, C.S., Leventer, A., Hogan, K., Cartigny, M., Rosenheim, B.E., Kuhn, G., Larter, R.D., (in press). History of Anvers-Hugo Trough, western Antarctic Peninsula shelf, since the Last Glacial Maximum. Part II: Palaeo-productivity and palaeoceanographic changes during the Last Glacial Transition.
- Rosenheim, B.E., Day, M.B., Domack, E., Schrum, H., Benthien, A., Hayes, J.M., 2008. Antarctic sediment chronology by programmed-temperature pyrolysis: methodology and data treatment. *G-cubed* 9.
- Rosenheim, B.E., Santoro, J.A., Gunter, M., Domack, E.W., 2013. Improving antarctic sediment 14C dating using ramped pyrolysis: an example from the Hugo Island trough. *Radiocarbon* 55, 115–126.
- Scambos A, T, Bohlander A, J, Shuman A, C, Skvarca, P, 2004. Glacier acceleration and thinning after ice shelf collapse in the Larsen B embayment, Antarctica. *Geophysical Research Letters* 31 (18).
- Schoof, C., 2007. Ice sheet grounding line dynamics: steady states, stability, and hysteresis. *J. Geophys. Res.: Earth Surf.* 112.
- Siegert, M., Alley, R.B., Rignot, E., Englander, J., Corell, R., 2020. Twenty-first century sea-level rise could exceed IPCC projections for strong-warming futures. *One Earth* 3, 691–703.
- Simkins, L.M., Greenwood, S.L., Anderson, J.B., 2018. Diagnosing ice sheet grounding line stability from landform morphology. *Cryosphere* 12, 2707–2726.
- Smith, J.A., Hillenbrand, C.-D., Larter, R.D., Graham, A.G.C., Kuhn, G., 2009. The sediment infill of subglacial meltwater channels on the West Antarctic continental shelf. *Quat. Res.* 71, 190–200.
- Smith, J.A., Hillenbrand, C.-D., Kuhn, G., Larter, R.D., Graham, A.G.C., Ehrmann, W., Moreton, S.G., Forwick, M., 2011. Deglacial history of the west antarctic ice sheet in the western Amundsen Sea embayment. *Quat. Sci. Rev.* 30, 488–505.
- Smith, J.A., Hillenbrand, C.-D., Kuhn, G., Klages, J.P., Graham, A.G.C., Larter, R.D., Ehrmann, W., Moreton, S.G., Wiers, S., Frederichs, T., 2014. New constraints on the timing of west antarctic ice sheet retreat in the eastern Amundsen Sea since the last glacial maximum. *Global Planet. Change* 122, 224–237.
- Smith, J.A., Andersen, T.J., Shortt, M., Gaffney, A.M., Truffer, M., Stanton, T.P., Bindschadler, R., Dutrieux, P., Jenkins, A., Hillenbrand, C.D., Ehrmann, W., Corr, H.F.J., Farley, N., Crowhurst, S., Vaughan, D.G., 2017. Sub-ice-shelf sediments record history of twentieth-century retreat of Pine Island Glacier. *Nature* 541, 77–80.
- Smith, J.A., Graham, A.G.C., Post, A.L., Hillenbrand, C.-D., Bart, P.J., Powell, R.D., 2019. The marine geological imprint of Antarctic ice shelves. *Nat. Commun.* 10, 5635.
- Subt, C., Fangman, K.A., Wellner, J.S., Rosenheim, B.E., 2016. Sediment chronology in Antarctic deglacial sediments: reconciling organic carbon 14C ages to carbonate 14C ages using Ramped Pyrolysis. *Holocene* 26, 265–273.
- Subt, C., Yoon, H.I., Yoo, K.-C., Lee, J.J., Leventer, A., Domack, E., Rosenheim, B., 2017. Sub-ice shelf sediment geochronology utilizing novel radiocarbon methodology for detrital-rich sediments. *G-cubed* 18, 1404–1418.
- Whitehouse, P.L., Bentley, M.J., Le Brocq, A.M., 2012a. A deglacial model for Antarctica: geological constraints and glaciological modelling as a basis for a new model of Antarctic glacial isostatic adjustment. *Quat. Sci. Rev.* 32, 1–24.
- Whitehouse, P.L., Bentley, M.J., Milne, G.A., King, M.A., Thomas, I.D., 2012b. A new glacial isostatic adjustment model for Antarctica: calibrated and tested using observations of relative sea-level change and present-day uplift rates. *Geophys. J. Int.* 190, 1464–1482.
- Witus, A.E., Braneky, C.M., Anderson, J.B., Szczuciński, W., Schroeder, D.M., Blankenship, D.D., Jakobsson, M., 2014. Meltwater intensive glacial retreat in polar environments and investigation of associated sediments: example from Pine Island Bay, West Antarctica. *Quat. Sci. Rev.* 85, 99–118.
- Wu, S., Kuhn, G., Diekmann, B., Lembke-Jene, L., Tiedemann, R., Zheng, X., Ehrhardt, S., Arz, H.W., Lamy, F., 2019. Surface sediment characteristics related to provenance and ocean circulation in the Drake Passage sector of the Southern Ocean. *Deep Sea Res. Oceanogr. Res. Pap.* 154, 103135.
- Yokoyama, Y., Anderson, J.B., Yamane, M., Simkins, L.M., Miyairi, Y., Yamazaki, T., Koizumi, M., Suga, H., Kusahara, K., Prothro, L., Hasumi, H., Southon, J.R., Ohkouchi, N., 2016. Widespread collapse of the Ross ice shelf during the late Holocene. *Proc. Natl. Acad. Sci. Unit. States Am.* 113, 2354.
- Yoon, H.I., Woo Han, M., Park, B.-K., Oh, J.-K., Soon-Keun, C., 1997. Glaciomarine sedimentation and palaeo-glacial setting of Maxwell Bay and its tributary embayment, Marian Cove, south Shetland Islands, west Antarctica. *Mar. Geol.* 140, 265–282.
- Yoon, H.I., Park, B.-K., Kim, Y., Kang, C.Y., 2002. Glaciomarine sedimentation and its paleoclimatic implications on the Antarctic Peninsula shelf over the last 15 000 years. *Palaeogeogr. Palaeoclimatol. Palaeoecol.* 185, 235–254.